ELECTRICAL AND MAGNETIC PROPERTIES

Transmission of Microwaves through Magnetic Metallic Nanostructures

A. B. Rinkevich[a], *, E. A. Kuznetsov[a, b], M. A. Milyaev[a], L. N. Romashev[a], and V. V. Ustinov[a]

[a]*Mikheev Institute of Metal Physics, Ural Branch, Russian Academy of Sciences, Ekaterinburg, 620108 Russia*
[b]*Russian State Vocational Pedagogical University, Ekaterinburg, 620012 Russia*
*e-mail: rin@imp.uran.ru

Abstract—The penetration of decimeter, centimeter, and millimeter electromagnetic waves through magnetic metallic nanostructures is considered in this work. Detailed information on the microwave giant magnetoresistive effect is presented. The manifestations of ferromagnetic and spin-wave resonances upon the transmission of microwaves through nanostructures are considered.

Keywords: metallic nanostructures, giant magnetoresistive effect, microwaves

INTRODUCTION

The rapid development of physics of metallic nanostructures began with the discovery of the giant magnetoresistive effect [1, 2]. This effect is observed in metallic nanostructures with at least two layers in which the magnetic moments are ferromagnetically ordered. Adjacent ferromagnetically ordered layers are separated by a non-ferromagnetic layer: a spacer. The thickness of the spacer is such that the adjacent ferromagnetic layers are coupled by exchange interaction. In nanostructures of different types (superlattices, spin valves, three-layer nanostructures, etc.), a different magnetic structure is realized that can be controlled by a magnetic field. The control of the electron spin in structures of reduced dimension is the subject of a modern field of science: spintronics [3−6]. The strong dependence of the electrical resistance of metallic nanostructures on the magnetic field quickly found practical application in many fields of technology, primarily in sensors and magnetoresistive memory devices. Therefore, the question immediately arose about the frequencies to which the giant magnetoresistive effect (GMR) can be realized and whether it can be realized in the microwave range and in optics. The answer to these questions was given in subsequent works. The fact that the GMR effect is realized with microwaves was established in [7, 8], and it was proposed in [9] to apply a method of transmission of microwaves through a nanostructure, which proved to be very effective. This effect in the microwave frequency range has been called the "microwave giant magnetoresistive effect" (µGMR). The GMR effect was also observed for infrared radiation [10]. In this review, we will focus mainly on the specifics of the µGMR in relation to decimeter, centimeter, and millimeter waves, i.e., to frequencies from ~0.5 to ~100 GHz. A review of early works on the µGMR was published in 2009 [11]. For more than ten years since then, new lines of research in this area have emerged and substantially new experimental material has been accumulated.

The structure of this review is as follows. First, we present the results on the interlayer exchange interaction and the "usual" GMR, i.e., GMR measured at a direct or low-frequency current. Then, we give some information on the growth and certification of metallic nanostructures and on their magnetic and magnetoresistive properties. These issues are related to the main topic of this review, and the presentation of them here is far from being complete. The purpose of discussing them in this review is to give general understanding of these problems and to provide the necessary references. Next, we disclose the physics of the microwave transmission method, and indicate the parameters of the nanostructure on which the transmitted and reflected signals depend and give a brief description of the equipment used to implement the method. In section "Transmission of microwaves through metallic nanostructures of different types. Microwave magnetoresistive effect" we present the main experimental results obtained to date by the microwave transmission method. In the subsequent sections, we describe the results of studying the µGMR in several special cases, namely, in the case of reflection of microwaves from a nanostructure and the microwave magnetoresistive effect when a current flows across the plane of the nanostructure layers. Next, we present the results on the ferromagnetic resonance and spin-wave resonance observed in nanostructures along with the µGMR. The µGMR effect

on the microwave refractive index has been studied quite recently.

1. INTERLAYER EXCHANGE INTERACTION

In this section, we will present necessary information on the interlayer exchange interaction in nanostructures. The main types of magnetic ordering of layers in nanostructures will be indicated, the concept of bilinear and biquadratic exchange will be given, and exchange constants will be introduced.

For a phenomenological description of the magnetic and magnetoresistive properties of superlattices, the following expression for the exchange energy of two ferromagnetic layers separated by a spacer is used:

$$E_{ex} = -J_1 \frac{(\mathbf{M_1 M_2})}{\mathbf{M_1 M_2}} - J_2 \frac{(\mathbf{M_1 M_2})^2}{(\mathbf{M_1 M_2})^2}, \qquad (1)$$

where $\mathbf{M}_1$ and $\mathbf{M}_2$ are the magnetizations of the ferromagnetic layers and J_1 and J_2 are the parameters of the bilinear and biquadratic exchange interaction. The value and the sign of the exchange constants in (1) depend on the layer thickness. In the absence of an external magnetic field, various types of magnetic ordering of adjacent ferromagnetic layers are possible: parallel, antiparallel, and noncollinear [12]. A microscopic theory of interlayer exchange interaction was developed in [13]. The exchange parameter has an oscillating dependence on the thickness of the nonmagnetic interlayer d_n, as in the Ruderman−Kittel-Kasuya−Yosida indirect exchange model [14−16]. In this model, the exchange parameter depends on the spacer thickness as follows: $J_1 \sim \sin(2k_F d_n)/d_n^2$, where k_F is the Fermi wavenumber in the spacer material. Depending on d_n, the sign of the exchange parameter can be either positive or negative. In the first case, the ordering of adjacent ferromagnetic layers is parallel and, in the second case, antiparallel. The first maximum of J_1 is usually found in the spacer at a depth of about 1 nm, and the second maximum, 2−2.2 nm.

2. GIANT MAGNETORESISTIVE EFFECT

The giant magnetoresistive effect (GMR) was discovered independently by Fert and Grünberg and their co-authors in $[Fe/Cr]_n$ superlattices [1, 2]. The effect consists in a significant, by tens of percent, reduction in the electrical resistance of superlattices when a magnetic field is applied. This effect was studied in superlattices made of various metals. The role of ferromagnets is played by iron, nickel, cobalt, and their alloys, and the spacer material are metals V, Cu, Ag, Cr, Au, Mo, Ru, Rh, Re, and Ir. The general objective of the research was to create nanostructures with the maximum GMR and a low magnetic field for the saturation of the effect. Record-high values of magneto-

resistance were obtained for Co/Cu and CoFe/Cu superlattices [15, 17, 18]. Many studies have been performed on superlattices and other nanostructures of the Fe/Cr system. At present, practical use requires nanostructures with a high maximum magnetoresistance, in particular, the CoFe/Cu and NiFe/Cu systems [19, 20].

The physical cause of the giant magnetoresistance of metallic nanostructures is spin-dependent scattering of conduction electrons. The highest magnetoresistance is realized in ferromagnetic metal/non-ferromagnetic metal pairs with the highest asymmetry of spin-dependent scattering [21]. Most often, experiments on measuring GMR are conducted in a variant in which the electric current flows in the plane of the nanostructure: this is the current-in-plane (CIP) geometry. Some works use a different geometry: current-perpendicular-to-plane (CPP) [22, 23]. In this geometry, the electron drift creating the electric current is perpendicular to the layers. As a result, the transition of electrons from layer to layer occurs more often and, at the boundaries of the layers, the accumulation of spins takes place. In the CPP geometry, the GMR effect is greater than in the CIP geometry. The theoretical description of the GMR effect for various directions of current in the CIP geometry was carried out in [24−26], and, in the CPP geometry, in [27]. A semiclassical theory of the GMR, unified for the CIP and CPP configurations, is presented in [28]. Examples of magnetoresistive dependences for nanostructures of various types will be given below, in Section 4.

3. GROWTH AND CERTIFICATION OF METALLIC NANOSTRUCTURES

The GMR effect is realized in nanostructures in which adjacent ferromagnetic layers are coupled by exchange interaction. Therefore, the layer thickness should be from tenths of nanometers to several nanometers. The main methods for obtaining metallic nanostructures with such thin layers are molecular beam epitaxy and magnetron sputtering [29]. Molecular beam epitaxy makes it possible to obtain single-crystal samples. To obtain the maximum GMR, the spacer thickness at the first maximum of the effect is selected to be about 0.9−1.2 nm. To obtain a nanostructure with a lower saturation field, the thickness of the spacer at the second maximum of GMR, 2.0−2.2 nm, is chosen. The top layer of the nanostructure is made of a corrosion-resistant metal such as chromium or tantalum. The magnetron sputtering method makes it possible to quickly produce multilayer films with a sufficiently high quality of the layered structure. This method makes it possible to sputter targets of complex composition, which makes it possible to create superlattices based on double and ternary ferromagnetic alloys, as well as complex nonmagnetic and antiferromagnetic alloys. Magnetron sputtering is used to obtain polycrystalline nanostructures. The
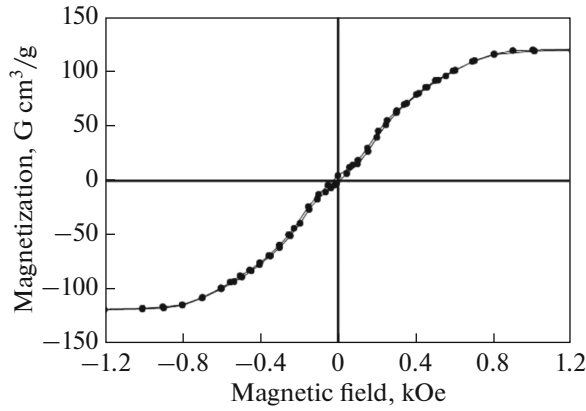
Fig. 1. Magnetization of a $(100)\mathrm{MgO}/[\mathrm{Fe}_{0.82}\mathrm{Ni}_{0.18}(1.03)/\mathrm{V}(1.9)]_{100}/\mathrm{Pd}(6)$ superlattice.

Fig. 2. Magnetization of superlattices and their approximation.

structure of ferromagnetic layers and nonmagnetic spacers depends on the composition, thickness, and technology of buffer preparation [30, 31].

Let us list the main methods for characterizing finished nanostructures. Information on the structure, frequency, and the state of the interfaces is provided by electron microscopy, as well as X-ray and neutron scattering methods. The superlattice period, i.e., the total thickness of the ferromagnetic layer and spacer is determined by small-angle X-ray diffraction. X-ray diffraction makes it possible to determine the type of crystal structure, the lattice parameters, and the presence and orientation of the texture. Electron microscopy makes it possible to determine whether a sample is a single crystal or a pseudo single crystal. In the latter case, it is possible to determine the lateral sizes of crystallites and the state of the boundaries between them. It is also possible to determine the crystallographic orientation of crystallites and other characteristics of the structure. Neutron diffraction methods are used to decipher the magnetic structure of superlattices [32, 33]. Scanning probe microscopy techniques such as tunneling microscopy and atomic force microscopy are used to characterize the surface relief of nanostructures. The domain structure is investigated by scanning magnetic force microscopy.

4. MAGNETIC AND MAGNETORESISTIVE PROPERTIES OF METALLIC NANOSTRUCTURES

In this section, we will describe methods for studying the magnetic and magnetoresistive properties of metallic nanostructures, as well as the measurement conditions (temperatures, fields, and measured quantities, as well as their use for analyzing microwave properties). Characteristic magnetization curves and magnetoresistive dependences for various types of nanostructures will be presented.
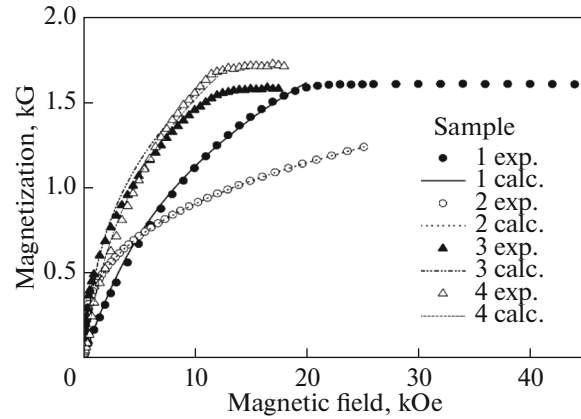
It is advisable to measure the magnetic properties using a SQUID magnetometer. Since the total thickness of the ferromagnetic layers is small and ranges from a few to one-two hundred nanometers, the contribution of a dielectric substrate several tenths of a millimeter thick is very significant and should be taken into account. Figure 1 shows the magnetization curve of a $(100)\mathrm{MgO}/[\mathrm{Fe}_{0.82}\mathrm{Ni}_{0.18}(1.03)/\mathrm{V}(1.9)]_{100}/\mathrm{Pd}(6)$ superlattice for the direction of the magnetic field along the [100] axis of the substrate [34]. In the superlattice in the absence of an external magnetic field, there is a parallel ordering of the adjacent $\mathrm{Fe}_{0.82}\mathrm{Ni}_{0.18}$ layers.

Figure 2 shows the magnetization curves of four samples of Fe/Cr superlattices, the layer thickness of which is given in Table 1. The table also presents some characteristics of the magnetization curves: saturation magnetization M_s and saturation field H_s.

The magnetization curves $M(H)$ shown in Fig. 2, for not too weak magnetic fields, can be approximated by a third-degree polynomial as an implicit function of H:

$$H = AM + BM^3, \quad H \leq H_{\mathrm{s}},$$
$$M = M_{\mathrm{s}}, \quad H > H_{\mathrm{s}}. \tag{2}$$

The possibility of approximation (2) is due to the form of expression (1) for the exchange energy in the biquadratic exchange model [35]. For a superlattice with an infinite number of periods, the approximation parameters A and B in formula (2) are expressed via the exchange constants J_1 and J_2:

$$A = \frac{4J_1 - 8J_2}{d_{\mathrm{FM}}M_{\mathrm{s}}^2}, \quad B = \frac{16J_2}{d_{\mathrm{FM}}M_{\mathrm{s}}^4}, \tag{3}$$

where d_{FM} is the thickness of the iron layers. The interlayer exchange constants calculated from the magnetization curves for several superlattices are presented in Table 1. The data obtained are in good agreement with

Table 1. Characteristics of samples

No.	Sample	M_s, kG	H_s, kOe	J_1, erg/cm^2	J_2, erg/cm^2
1	[Cr(1.1)/Fe(1.06)]$_{30}$/Cr(8)/MgO	1.62	20	0.75	0.12
2	[Cr(1.1)/Fe(0.9)]$_{40}$/Cr(8.5)/MgO	1.18	25	0.35	0.17
3	[Cr(1.2)/Fe(2.3)]$_{16}$/Cr(7.7)/MgO	1.7	12.6	0.76	0.24
4	[Cr(1.3)/Fe(2.4)]$_8$/Cr(8.2)/MgO	1.65	12.0	0.82	0.18

the results of [36], where, for a [Fe(2.1)/Cr(1.04)]$_{12}$ superlattice, the values J_1 = 0.4 erg/cm^2 and J_2 = 0.23 erg/cm^2 were obtained. Information on the exchange constants of superlattices of the [Fe/Cr]$_n$ system is given in [37−39].

The electrical resistance of samples of nanostructures is measured by the four-contact method. It is convenient to characterize the magnitude of the effect by the relative magnetoresistance

$$r = [R(H) - R(0)]/R(0), \qquad (4)$$

where $R(H)$ is the resistance of the sample in a magnetic field H. At room temperature, r reaches tens of percent. Magnetoresistive dependences for several [Fe/Cr]$_n$ superlattices are shown in Fig. 3. As a rule, the giant magnetoresistance of metallic superlattices is negative. The magnetoresistance is saturated in strong fields. In superlattices with parallel ordering of adjacent and nearby layers, the saturation field H_s is relatively small. In such superlattices, the relative magnetoresistance at saturation is no more than a few percent.

The relative magnetoresistance defined by formula (4) is close to zero if $R(H) \approx R(0)$ and close to −1 if $R(H) \ll R(0)$. In the latter case, it is more convenient to define r as
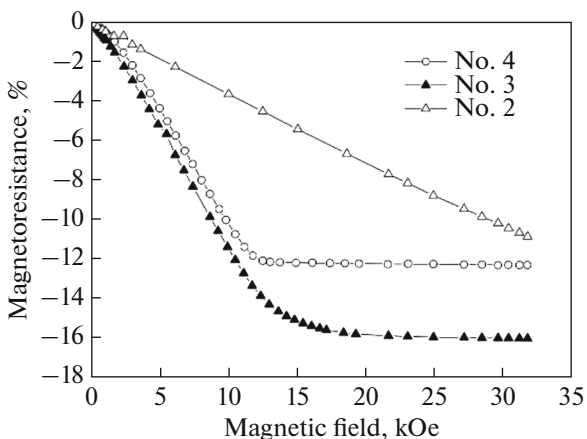
$$r = (R(H) - R_s)/R_s, \qquad (4a)$$

where R_s is the resistance in a magnetic saturation field. The results of measuring the magnetoresistance of two samples of superlattices of the (CoFe)/Cu system, prepared by magnetron sputtering, are shown in Fig. 4 [31, 40]. The highest magnetoresistance of 78% is possessed by the Ta(5)/RuCr(5)/[Co$_{88}$Fe$_{12}$(1.5)/Cu(0.95)]$_{24}$/Ta(5) sample (Fig. 4a). The spacer thickness for this sample is 0.95 nm, which is close to the first maximum of the GMR.

The magnetic saturation field for this sample is about 7.5 kOe. The Ta(5)/RuCr(5)/[Co$_{88}$Fe$_{12}$(1.3)/Cu(2.05)]$_8$/Co$_{88}$Fe$_{12}$(1.3)/RuCr(3) sample (Fig.4b) also exhibits a very high magnetoresistance of about 25%, and saturation occurs in much weaker fields of about 400 Oe. For this sample, the spacer thickness falls on the second maximum.

5. MICROWAVE TRANSMISSION METHOD

Studying the high-frequency characteristics of magnetic nanostructures is one of the important tasks of spintronics and magnonics. Both planar nanostructures and laterally limited objects are investigated. The use of spintronic effects to control the propagation of spin waves provides new opportunities for the implementation of nano-oscillators, as well as for the conversion of spin currents into electric currents and vice versa [41−43]. In this section, we will present schematics of methods for measuring the transmission of microwaves through nanostructures and list the measured parameters. A theoretical analysis of the method will be given, limiting cases will be considered, and a comparison of the techniques used by different research groups will be made.

The μGMR effect was discovered using the magnetic resonance technique [7, 8]. In the traditional form of this method, the sample is placed in a microwave resonator, and changes in the resonant frequency and the Q-factor are recorded [44]. As a rule, measurements are carried out in a modulation mode, when an alternating magnetic field is superimposed on a constant one. Therefore, the received signal is proportional to the derivative of the measured quantity with respect to the magnetic field. It was found in [7] that in addition to the ferromagnetic resonance lines, a three-layer Fe/Cr nanostructure exhibits anomalies,

Fig. 3. Magnetoresistive dependence of superlattices nos. 2–4.

the position of which does not depend on the frequency, but corresponds to a field with the steepest magnetoresistive characteristic. The authors of [7] related these anomalies to the Joule loss in the metallic nanostructure and, therefore, to the GMR. This technique does not allow us to investigate all the important magnetoresistive characteristics. In particular, it is difficult to quantify the microwave magnetoresistive dependence. Nevertheless, this technique has been used for experimental research for many years, not least due to the fact that measurements can be performed on standard certified equipment. In particular, this method was used in [45−47]. A significant disadvantage of this technique is that the microwave frequency is fixed due to the use of a high-Q resonator. The use of a modern network analyzer makes it possible to work not with a resonator, but with a segment of a transmission line, e.g., a strip line, and perform measurements in a frequency range [48, 49].

The state of the art study of the µGMR effect began with the work [9], in which the technique using the penetration of microwaves through a nanostructure was successfully applied. The penetration of microwaves through thin metal films was considered in the literature earlier [50]. It was shown in [9] that the relative change in the microwave transmission coefficient is equal to the relative magnetoresistance measured at direct current. It should be noted that the transmission of microwaves through thin metal films is used to find the conductivity at a known film thickness, or, on the contrary, to determine the film thickness at a known conductivity [51].

A consistent presentation of the microwave transmission method for studying µGMR is given in [11, 52, 53]. The issues of the joint study of the ferromagnetic resonance (FMR) and µGMR are considered in [54]. An original technique for studying the µGMR, applicable to the case of decimeter waves, was proposed in [55]. A modification of the transmission method for the quantitative measurement of microwave magnetoresistance at centimeter and millimeter wavelengths is considered in [56]. It was found that the µGMR effect can be observed in a wave reflected from a nanostructure [57−59]. This version of the technique is detailed below, in Section 7. The µGMR effect on infrared radiation is considered in [60−63]. Below, we will consider a technique using the transmission of microwaves through a metal nanostructure and discover what information about the properties of the nanostructure can be extracted from such measurements. The presentation will follow [9, 54, 64].

Microwave measurements are performed at frequencies f from ~8 to ~70 GHz using equipment capable of producing microwaves and measuring their amplitude or power, such as a vector or scalar network analyzer, or measuring the frequency response function (FRF) and standing wave ratio (SWR).
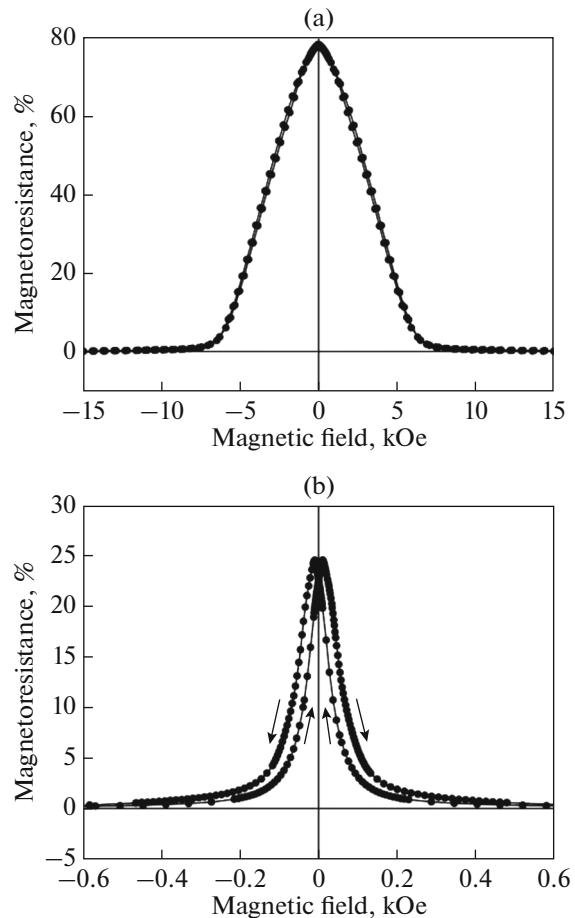

Fig. 4. Giant magnetoresistive effect in [CoFe/Cu]$_n$ superlattices with record-high magnetoresistance: (a) Ta(5)/RuCr(5)/[Co$_{88}$Fe$_{12}$(1.5)/Cu(0.95)]$_{24}$/Ta(5) sample and (b) Ta(5)/RuCr(5)/[Co$_{88}$Fe$_{12}$(1.3)/Cu(2.05)]$_8$/Co$_{88}$Fe$_{12}$(1.3)/RuCr(3) sample.

The sample is placed in a mandrel with the same dimensions as the flange of a standard waveguide and with the same mounting holes [11, 59, 64]. A mandrel with a sample is placed between the flanges of a standard rectangular waveguide across it so as to completely cover the cross section. The gaps between the sample and the mandrel are filled with conductive glue to prevent spurious leakage of the field around the sample. A possible schematic diagram of microwave measurements is shown in Fig. 5.

The output signal from the oscillator of the frequency response meter is fed to the coaxial-waveguide junction that excites the TE$_{10}$ wave in the waveguide *1*. The waveguide of the selected section is used in the frequency range in which only the TE$_{10}$ mode can propagate. The wave incident on nanostructure sample *4* partially reflects from it and partially passes through. Through directional couplers *3*, the transmitted and reflected waves fall on the inputs of the frequency response meter. The transmitted wave partially
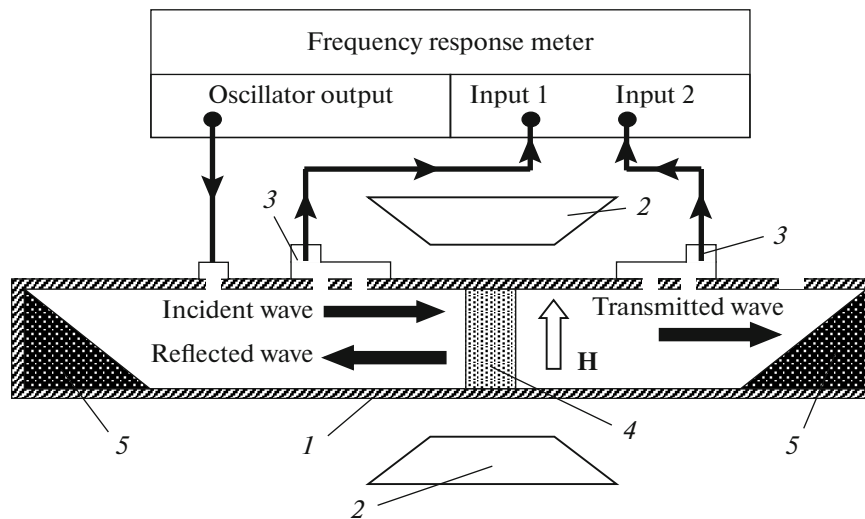
Fig. 5. Schematic diagram of microwave measurements: (*1*) waveguide, (*2*) electromagnet, (*3*) directional coupler, (*4*) sample, and (*5*) absorber.
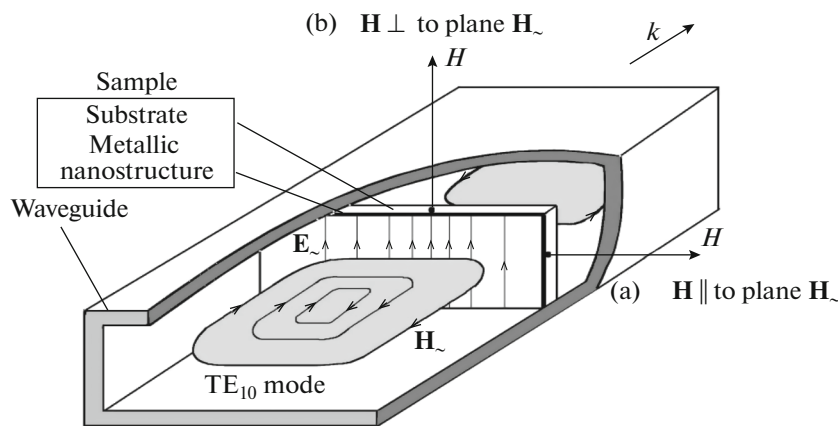

Fig. 6. Schematics of field orientation when placing a nanostructure sample in a waveguide.

falls on the absorber *5* to prevent unwanted reflection. The sample of a metallic nanostructure creates a significant inhomogeneity in the waveguide that is expressed in a high value of SWR ≫ 1. Therefore, it is very important that the sample be the only significant inhomogeneity in the transmission line. A magnetic field **H** with a strength up to 12 kOe is generated by the electromagnet *2*. The magnetic field lies in the plane of the sample, and two orientations of the constant field can be realized: $\mathbf{H} \parallel \mathbf{H}_\sim$ and $\mathbf{H} \perp \mathbf{H}_\sim$, where $\mathbf{H}_\sim$ is the microwave magnetic field vector. The layout of the fields is shown in Fig. 6. The microwave electric field $\mathbf{E}_\sim$ lies in the plane of the sample.

The absolute value of the transmission, *D*, and the reflection, *R*, coefficients and their changes in the magnetic field are measured. The relative changes in the coefficients are defined as $d_\mathrm{m} = [|D(H)| - |D(0)|]/|D(0)|$, where

$|D(H)|$ is the absolute value of the transmission coefficient and $r_m = [|R(H)| - |R(0)|]/|R(0)|$, where $|R(H)|$ is the absolute value of the reflection coefficient.

Based on the analysis of the propagation of electromagnetic waves in a magnetized ferromagnet carried out in [65], let us describe the scheme of calculating the transmission and reflection coefficients. In this version of the calculation, it will be taken into account that the μGMR effect influences the microwave characteristics *D* and *R* through the conductivity of the nanostructure, skin depth, and complex wavenumber, while the resonant changes in the transmission coefficient are caused by the resonance in the effective permeability of the ferromagnetic film. It should be noted that a multilayer inhomogeneous nanostructure in the calculation is replaced with a plate made of a homogeneous ferromagnetic metal of the same thickness and

with effective parameters: conductivity and static and dynamic permeabilities [66].

The complex wavenumber $k = k' - ik''$ of an electromagnetic wave is defined by the formula

$$k = \frac{\sqrt{\mu_{eL}} - i\sqrt{\mu_{eR}}}{\delta}. \tag{5}$$

Let us determine the quantities μ_{eL} and μ_{eR} entering into expression (5). We write the equation of motion for the magnetization in the Gilbert form:

$$\frac{\partial \mathbf{M}}{\partial t} = -\gamma \mathbf{M} \times \mathbf{H} + \frac{\alpha}{M} \mathbf{M} \times \frac{\partial \mathbf{M}}{\partial t}, \tag{6}$$

where $\mathbf{M}$ is the magnetization vector, $\mathbf{H}$ is the magnetic field strength vector, α is the dissipation parameter related to the Gilbert constant G by the formula $\alpha = \dfrac{G}{\gamma M_s}$. Equation (6) can be linearized under the assumption that the variable (microwave) components of the magnetic field strength and magnetization in it are small. As a result, we have the following expression for the high-frequency permeability tensor:

$$\ddot{\mu} = \begin{pmatrix} \mu & i\mu_a & 0 \\ -i\mu_a & \mu & 0 \\ 0 & 0 & \mu_\parallel \end{pmatrix}, \tag{7}$$

where $\mu = 1 + 4\pi\chi$, $\mu_a = 4\pi\chi_a$, and $\mu_\parallel = 1 + 4\pi\chi_\parallel$. Here,

$$\chi = \chi' - i\chi'' = \gamma M$$
$$\times \frac{\omega_H \left[\omega_H^2 - \left(1 - \alpha^2\right)\omega^2 \right] - i\alpha\omega\left[\omega_H^2 + \left(1 + \alpha^2\right)\omega^2 \right]}{D}, \tag{8a}$$

$$\chi_a = \chi_a' - i\chi_a''$$
$$= \gamma M \omega \frac{\left[\omega_H^2 - \left(1 + \alpha^2\right)\omega^2 \right] - i2\alpha\omega\omega_H}{D}, \tag{8b}$$

$$\chi_\parallel = -\frac{i\alpha\gamma M}{\omega - i\alpha\omega_H}, \tag{8c}$$

where ω is the angular frequency, $D = [\omega_H^2 - \left(1 + \alpha^2\right)\omega^2]^2 + 4\alpha^2\omega^2\omega_H^2$, and $\omega_H = \gamma H$. The magnetic field $\mathbf{H}$ is parallel to the axis $0z$.

The effective permeability for an electromagnetic wave under the condition that $\mathbf{k} \perp \mathbf{H}$ is defined by the ratio

$$\mu_{eff} = \mu - \frac{\mu_a^2}{\mu}. \tag{9}$$

The wavenumber of a plane electromagnetic wave propagating in a ferromagnetic medium is defined by the formula $k = \dfrac{\omega}{c}\sqrt{\varepsilon_{eff}\mu_{eff}}$, where the effective permittivity ε_{eff} and effective permeability μ_{eff} are com-

plex quantities: $\varepsilon_{eff} = \varepsilon_{eff}' - i\varepsilon_{eff}''$ and $\mu_{eff} = \mu_{eff}' - i\mu_{eff}''$. For a conductive ferromagnetic plate, $\varepsilon_{eff}' \ll \varepsilon_{eff}'' = \dfrac{4\pi\sigma}{\omega}$. In this case, the wavenumber is

$$k = \frac{\omega}{c}\sqrt{-i\frac{2\pi\sigma}{\omega}\left(\mu_{eff}' - i\mu_{eff}''\right)} = \frac{\sqrt{2}}{\delta}\sqrt{-i\mu_{eff}' - \mu_{eff}''}.$$

The square root of a complex quantity is a multivalued function. Therefore, when finding a complex wavenumber, it is necessary to choose the solution that corresponds to the principle of limiting absorption. According to [65], this gives the following result:

$$k = k' - ik'' = \frac{\sqrt{|\mu_{eff}| - \mu_{eff}''} - i\sqrt{|\mu_{eff}| + \mu_{eff}''}}{\delta}. \tag{10}$$

From (10), using the notation $\mu_{eL} = |\mu_{eff}| - \mu_{eff}''$ and $\mu_{eR} = |\mu_{eff}| + \mu_{eff}''$, we obtain formula (5).

The impedance of a ferromagnetic medium is defined by the relationships $Z = \dfrac{\omega\mu_{eff}}{kc} = \dfrac{kc}{\omega\varepsilon_{eff}} = \dfrac{ikc}{4\pi\sigma}$, from which, using formula (5), we can obtain the expression

$$Z = \frac{c}{4\pi}\frac{\sqrt{\mu_{eR}} + i\sqrt{\mu_{eL}}}{\sigma\delta}. \tag{11}$$

The longitudinal wavenumber for the TE_{10} mode of a rectangular waveguide for regions filled with a dielectric medium with a relative permittivity ε_s and a relative permeability μ_s, is determined by the expression [67]

$$\Gamma = \frac{\omega}{c}\sqrt{\varepsilon_s\mu_s - \left(\frac{\pi c}{\omega a}\right)^2}, \tag{12}$$

where a is the width of the waveguide. The impedance of an H-wave is expressed as $Z = \dfrac{\omega\mu}{c\Gamma}$. Substituting formula (12) into this expression, we obtain

$$Z = \mu_s\left[\varepsilon_s\mu_s - \left(\frac{\pi c}{\omega a}\right)^2\right]^{-\frac{1}{2}}. \tag{13}$$

Let us consider the transmission of an electromagnetic wave through a system consisting of a conductive ferromagnetic layer with a thickness d and a dielectric substrate with a thickness d_s (region 2), separating two half-spaces. We assume that, in both of these half-spaces, $\varepsilon_s = 1$ and $\mu_s = 1$. We denote the corresponding wavenumber and the impedance as Γ_1 and Z_1. According to formulas (12) and (13), we obtain

$$\Gamma_1 = \frac{\omega}{c}\sqrt{1 - \left(\frac{\pi c}{\omega a}\right)^2} \text{ and } Z_1 = \left[1 - \left(\frac{\pi c}{\omega a}\right)^2\right]^{-\frac{1}{2}}. \text{ Similarly,}$$

for a dielectric layer with a thickness d_s and a parameter $\mu_s = 1$, we can introduce the notations $\Gamma_2 = \dfrac{\omega}{c}\sqrt{\varepsilon_s - \left(\frac{\pi c}{\omega a}\right)^2}$ and $Z_2 = \left[\varepsilon_s - \left(\frac{\pi c}{\omega a}\right)^2\right]^{-\frac{1}{2}}$. The corre-

sponding characteristics Γ_3 and Z_3 of the conductive ferromagnetic layer with a thickness d are specified by formulas (5) and (11).

The transmission and reflection coefficients D and R depend on the ratio of the impedances of the nanostructure, Z_m, and the ambient medium, Z_1, as well as on the ratio of the nanostructure thickness d and the skin depth δ. Under the condition of the normal skin effect, the impedance of the metallic nanostructure in the effective medium approximation is $Z_m = [(1 + i)/\delta]\rho$, where ρ is the electrical resistivity of the nanostructure, $\delta = (2\rho/\omega\mu\mu_0)^{1/2}$ is the skin depth, and μ is the relative dynamic differential permeability. The impedance of the waveguide in which the nanostructure is placed on the TE_{10} mode wave is determined by the formula [67]

$$Z = (m_0/e_0)^{1/2}\big/[(1 - (l/l_c)^2]^{1/2}, \qquad (14)$$

where $\lambda = c/f$ is the wavelength in vacuum and $\lambda_c = 2a$ is the critical wavelength of the TE_{10} mode wave. According to [67], the coefficients D and R of an electromagnetic wave can be expressed as

$$D = \frac{2Z_m}{2Z_m\cosh k_m d + Z\sinh k_m d},$$
$$R = -1 + \frac{2Z_m\cosh k_m d}{2Z_m\cosh k_m d + Z\sinh k_m d}, \qquad (15)$$

where k_m is the wavenumber in the conducting medium and $k_m = (1 + i)/\delta$. The impedance of the conducting nanostructure is lower than the impedance Z, $|Z_m| \ll Z$. If, in the denominator of Eqs. (15), $2Z_m\cosh k_m d \ll Z\sinh k_m d$, then the transmission and reflection coefficients are expressed as

$$D = \frac{2Z_m}{Z\sinh k_m d}, \quad R = -1 + \frac{2Z_m}{Z}\coth k_m d. \qquad (16)$$

In this limiting case, the coefficients D and R depend on the frequency, due to the frequency dispersion of the constants and the frequency dependence of the impedance of the waveguide, Z. This dependence of the impedance Z is weak, far from the cutoff frequency of the waveguide, $f_c = c/2a$. In particular, formula (16) implies the one-to-one correspondence, established in [9], between the GMR effect measured at a direct current and the relative change in the transmission coefficient if $\mu \approx 1$, i.e., the relationship

$$d_m = r. \qquad (17)$$

Formulas (15) are written for a thin metal plate. Metallic nanostructures are usually grown on dielectric substrates. Therefore, it is necessary to generalize formulas (15) to the case with a substrate. Let us use the expressions for the transmission and reflection coefficients of a three-layer system, found in [68]:

$$D = \frac{Z_1^{in} + Z_1}{Z_1^{in} + Z_2} \frac{Z_2^{in} + Z_2}{Z_2^{in} + Z_3} \frac{Z_3^{in} + Z_3}{Z_3^{in} + Z_1} \qquad (18)$$
$$\times \exp[-i(\varphi_2 + \varphi_3)],$$

$$R = \frac{Z_3^{in} - Z_1}{Z_3^{in} + Z_1}, \qquad (19)$$

where Z_n^{in} is the input impedance of the nth domain, $\varphi_n = k_n d_n$ is the phase shift of the wave arising after the wave passes through the nth domain, k_n is the wavenumber in the nth domain, and d_n is the thickness of the nth domain. The first domain is an empty waveguide, the second domain is a metallic nanostructure with $d_2 = d$, and the third domain is a dielectric substrate with $d_3 = d_s$. The input impedances are expressed as

$$Z_1^{in} = Z_1; \quad Z_2^{in} = Z_2\frac{Z_1 + iZ_2\tan\varphi_2}{Z_2 + iZ_1\tan\varphi_2};$$
$$Z_3^{in} = Z_2 \qquad (20)$$
$$\times \frac{Z_1(Z_2 - Z_3\tan\varphi_2\tan\varphi_3) + iZ_2(Z_2\tan\varphi_2 - Z_3\tan\varphi_3)}{Z_2(Z_3 - Z_2\tan\varphi_2\tan\varphi_3) + iZ_1(Z_3\tan\varphi_2 - Z_2\tan\varphi_3)}.$$

In formula (20), $Z_1 = Z$ is the impedance of the waveguide at a given frequency, $Z_2 = Z_m$ is the impedance of the metallic nanostructure, and Z_3 is the impedance of the substrate. The application of the above procedure to a system of several layers is considered in [69].

There are several more variations of the transmission method. One of them, in which radio frequency or microwave currents flow across the layers of the nanostructure, will be discussed below. In addition, there is a technique in which a nanostructure sample is parallel to the waveguide axis [70−72]. In this case, a traveling electromagnetic wave propagating along the nanostructure arises. Consideration of this technique is beyond the scope of this review. We only note that such an arrangement of the nanostructure can be used to measure high-frequency giant magnetoresistance [73] and to construct microwave devices [74].

6. TRANSMISSION OF MICROWAVES THROUGH METALLIC NANOSTRUCTURES OF DIFFERENT TYPES. MICROWAVE MAGNETORESISTIVE EFFECT

As noted above, the microwave giant magnetoresistive effect was discovered in [7]; the experiments were conducted on a magnetic resonance spectrometer. After the publication of [9], where the transmission method was successfully used, a significant number of studies on the µGMR were carried out. The current state of research was reviewed in [11] and in a brief

review [75]. In this section, we will present the experimental results on the transmission of microwaves through various types of metallic nanostructures: superlattices with solid layers, three-layer systems, and cluster-layered structures. The specificity of the transmission of waves through nanostructures made of different materials: Fe/Cr, Co/Cu, AgPt/Co, FeCo/Cu, and FeNi/V, will be considered. A comparison between the μGMR and GMR will be made. First of all, let us analyze formulas (15) from the standpoint of the accuracy of the fulfilment of relationship (17).

In the limiting case, when the inequality $2Z_m\cosh(k_m d) \ll Z\sinh(k_m d)$ in the denominator of Eq. (15) holds and equality (17) is satisfied, the relative change in the transmission coefficient in a magnetic field does not depend on the total thickness of the metal in the nanostructure. At the same time, there is such a dependence in Eqs. (15). Let us perform numerical calculations of the μGMR in the transition region, when $2Z_m\cosh(k_m d) \le Z\sinh(k_m d)$. The calculations will be performed for a nanostructure with high conductivity in zero field, $\sigma(0) = 1.26 \times 10^6$ S/m. We assume that the nanostructure has a magnetoresistance similar to that shown in Fig. 7a. The maximum magnetoresistance of −25% is achieved at magnetic saturation in fields above 8 kOe. The nanostructure was grown on a substrate with a thickness $d_s = 0.3$ mm and a permittivity $\varepsilon_s = 5.0$. We assume that the magnetoresistance remains the same as shown in Fig. 7a as the total thickness of the metal of the nanostructure d changes. The result of calculating μGMR by formula (15) for different thicknesses d of the metal in the nanostructure is shown in Fig. 7b. It can be seen that, at $d \ge$ 50 nm, the equality of μGMR and GMR is quite accurate; with decreasing thickness, at $d \sim$ 20 nm, μGMR decreases and the equality is satisfied only approximately; and a further decrease in d leads to a very significant decrease in μGMR.

In the reflected signal, the picture of changes is different. First, as d decreases, μGMR increases, reaches a maximum at $d = 3$ nm, and then decreases. The dependence of the maximum change in the transmission and reflection coefficients on the metal thickness d is shown in Fig. 7c. Let us now consider the results of experimental studies of μGMR for several superlattice systems.

Fe/Cr System

The Fe/Cr system has been studied in most detail, starting with [7−9]. A detailed description of the physical causes of the change in the transmission coefficient in a magnetic field is given in [52]. Examples of dependences of the transmission coefficient on the magnetic field at the μGMR for nanostructures of various types are given in [76].

Let us first consider the μGMR effect for superlattices with solid layers. In a $[Cr(1.8)/Fe(2.8)]_{12}/Cr(7.7)/MgO$
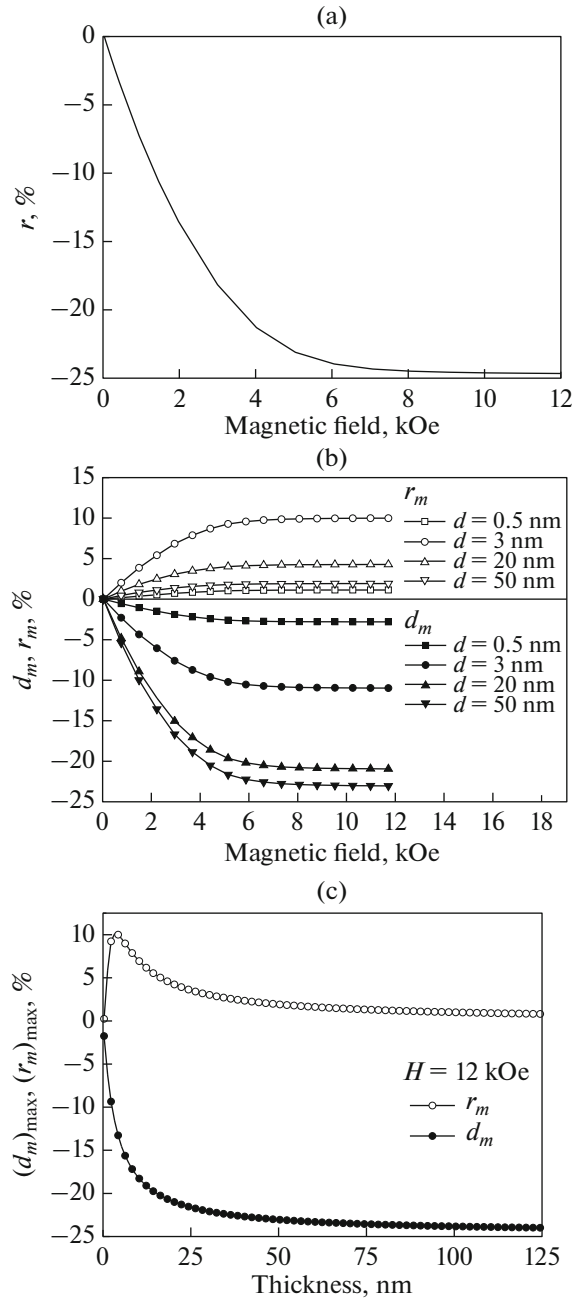

Fig. 7. Field dependence: (a) DC magnetoresistance of a nanostructure with conductivity $\sigma(0) = 1.26 \times 10^6$ S/m; (b) transmission and reflection coefficients at a frequency $f = 32$ GHz, calculated for several thicknesses of the nanostructure; and (c) relative changes in a field of 12 kOe vs. the thickness of the nanostructure.

superlattice with a saturation field of about 4.5 kOe, in addition to a monotonic decrease in the transmission coefficient, caused by the μGMR, a transmission minimum due to the FMR was observed. Figure 8 shows the dependences $d_m(H)$ measured at frequencies from 30 to 38 GHz. It should be noted that the nonresonant part of the relative change in the microwave
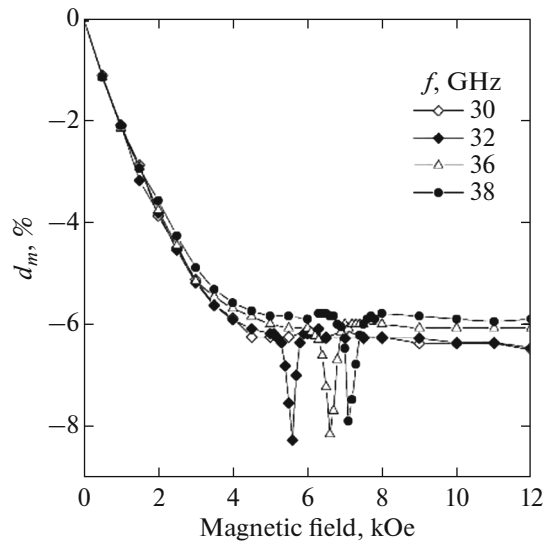
Fig. 8. Variation in the microwave transmission coefficient for a $[Cr(1.8)/Fe(2.8)]_{12}/Cr(7.7)/MgO$ sample in a constant magnetic field for the case of $\mathbf{H}\perp\mathbf{H}_\sim$ at various frequencies.

Fig. 9. Field dependences of static magnetoresistance (r) and microwave transmission coefficient (d_m) at a frequency of 36 GHz for the cases of $\mathbf{H}//\mathbf{H}_\sim$ and $\mathbf{H}\perp\mathbf{H}_\sim$ for multilayer Fe/Cr samples: (a) $[Cr(1.1)/Fe(0.9)]_{40}/Cr(8.5)/MgO$ superlattice; (b) cluster-layered $[Cr(1.1)/Fe(0.4)]_{50}/Cr(8.5)/MgO$ nanostructure.

transmission coefficient, caused by the μGMR, is somewhat lower than the relative magnetoresistance, which reaches −7.7% in saturation.

Investigations of microwave transmission for the cases of $\mathbf{H}//\mathbf{H}_\sim$ and $\mathbf{H}\perp\mathbf{H}_\sim$ were also carried out on a $[Cr(1.1)/Fe(0.9)]_{40}/Cr(8.5)/MgO$ superlattice with thin Fe layers (Fig. 9a) and on cluster-layered nanostructure $[Cr(1.1)/Fe(0.4)]_{50}/Cr(8.5)/MgO$ (Fig. 9b). For a sample with thin layers, a weak resonance minimum is observed at $\mathbf{H}\perp\mathbf{H}_\sim$. No resonant changes were observed in a cluster-layered Fe/Cr nanostructure. Figure 9 also shows the dependence of the magnetoresistive effect GMR. In all cases, outside the FMR region, an approximate equality of the μGMR and GMR is observed.

It was shown in [77] that the magnetoresistance of cluster-layered Fe/Cr nanostructures with thicknesses of the Fe layer below the percolation threshold depends linearly on an external magnetic field strength in a fairly wide range of fields and is almost independent of the direction of the field. Another feature of cluster-layered Fe/Cr nanostructures with Fe cluster layers is that the temperature coefficient of electrical resistivity can change sign, just as in alloys with the Kondo effect.

The magnetic, magnetoresistive, and high-frequency properties of Fe/Cr nanostructures with thicknesses of the Cr layer both above and below the percolation threshold were studied in [78]. The percolation threshold of Fe/Cr nanostructures grown by molecular beam epitaxy appears at layer thicknesses of ~(0.4–0.5) nm and strongly depends on the quality of the substrate surface. In nanostructures with thicknesses
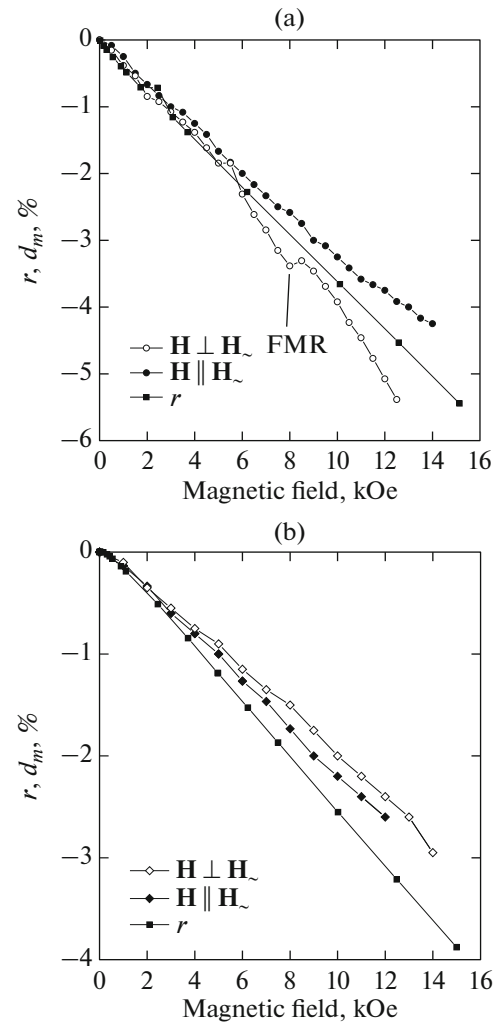
of the Cr layer below the percolation threshold, the μGMR is practically absent. In Fe/Cr superlattices with thin Cr layers, the microwave analogue of the giant magnetoresistance effect is observed regardless of whether the direction of the constant magnetic field $\mathbf{H}$ is parallel or perpendicular to the plane of the microwave magnetic field $\mathbf{H}_\sim$. The magnetoresistance of metallic multilayer Fe/Cr nanostructures is negative; the microwave transmission coefficient also decreases due to the presence of the μGMR effect in a magnetic field (see Fig. 10).

It can be seen from Fig. 10a that the relative change in the microwave transmission coefficient has a field dependence similar to the GMR.
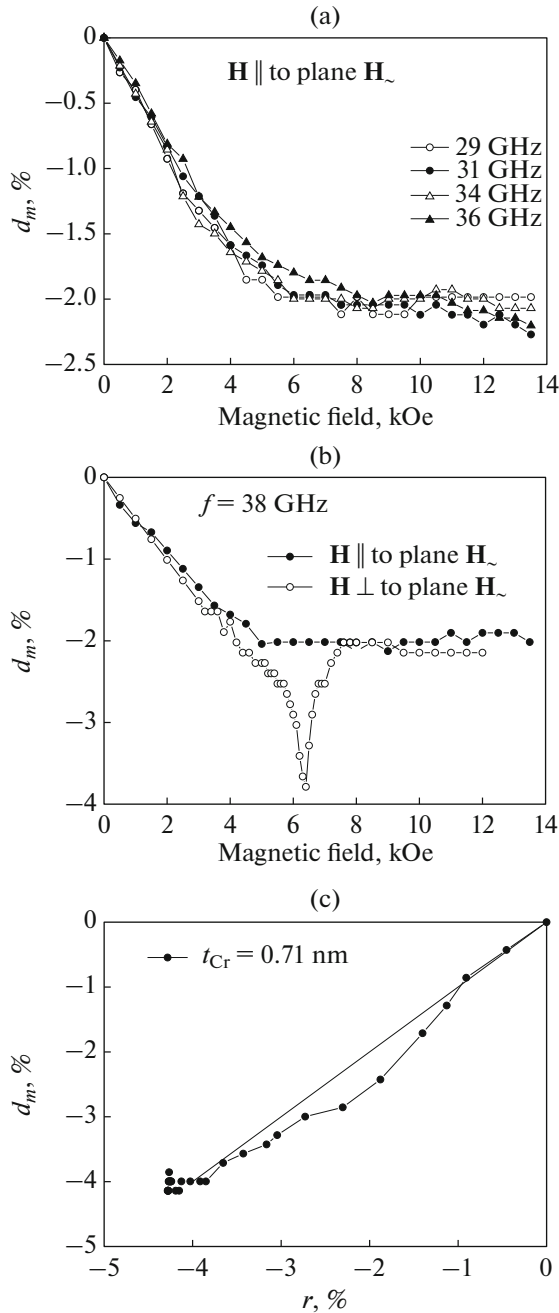
(a)

(b)

(c)

Fig. 10. (a) Field dependence of the transmission coefficient through a $[Cr(0.7nm)/Fe(2.6nm)]_{12}/Cr(6.5nm)/Al_2O_3$ nanostructure, measured at several frequencies for $\mathbf{H}//\mathbf{H}_\sim$; (b) microwave GMR and magnetic resonance for the same nanostructure; and (c) comparison of microwave magnetoresistance and DC magnetoresistance.

The observed changes in the transmission coefficient arising from the presence of the µGMR effect in the nanostructures under consideration have a weak frequency dependence.

Let us consider the frequency dependence of the µGMR for Fe/Cr superlattices. Figure 11 shows the frequency dependence of the relative change in
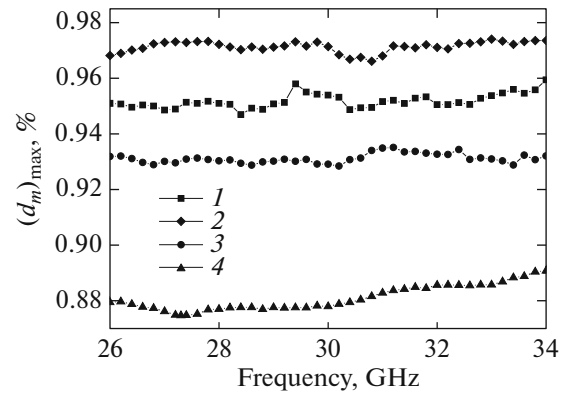

Fig. 11. Frequency dependence of the relative change in the transmission coefficient through the samples of Fe/Cr superlattices: (No. 1) $[Fe(2.3)/Cr\ (1.9)]_{12}/Cr(8)/Al_2O_3$; (No. 2) $[Fe(0.9)/Cr(1.1)]_{40}/Cr(8.5)/MgO$; (No. 3) $[Fe(0.4)/Cr(1.1)]_{50}/Cr(8.5)/MgO$; and (No. 4) $[Fe(2.3)/Cr\ (1.2)]_{16}/Cr\ (7.7)/MgO$.

the transmission coefficient $(d_m)_{max}$ through several samples of Fe/Cr superlattices with different thicknesses of the Fe and Cr layers, measured in a magnetic field of 12 kOe [79]. The field $H = 12$ kOe is chosen to achieve a state close to magnetic saturation. It can be seen from the figure that the frequency dependence of these changes is weak. As a rule, the changes in the microwave transmission coefficient are either equal to or slightly less than the relative magnetoresistance. The µGMR effect and measurements of the FMR and the magnetization curve were used in [36] to determine the numerical values of the bilinear and biquadratic constants of the interlayer exchange interaction. The results of this work are partially presented in Section 4.

Co/Cu System

The high-frequency magnetoresistance of Co/Cu nanostructures was studied in [55, 80]. In [80], the experimental technique was modified. The short side of the waveguide where the sample was located was made smaller, which slightly reduced the mismatch of the microwave transmission line. The measurements were carried out in a frequency range from 30 to 140 GHz with a $[Co(1.0)/Cu(1.7)]_{30}$ superlattice. At the highest frequencies, the microwave magnetoresistance was lower than GMR, $d_m < r$. However, the shape of the field dependence of the µGMR and GMR turned out to be the same.

The microwave magnetoresistance of Co/Cu nanostructures grown on single-crystal silicon substrates was studied in [55]. In this work, an original measurement technique was applied, suitable for frequencies in the decimeter-wavelength range. A sample in the form of a strip with a size of 0.3×6 mm was
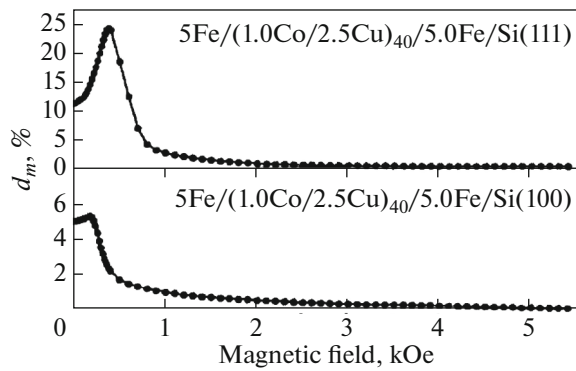
Fig. 12. Microwave magnetoresistance of Co/Cu nano-structures: data from [55].

Fig. 13. Frequency dependence of μGMR in Co/Cu nano-structures: data from [55].

placed in a loop antenna, and the real and imaginary parts of the impedance were measured. This technique measures the apparent magnetoresistance that includes the radiation loss. The dependence of the apparent magnetoresistance on the magnetic field for two crystallographic orientations of the substrate is shown in Fig. 12. It can be seen that the magnetoresistance at the maximum reaches 25%. This has been a record-high for the μGMR for many years. Figure 13 shows the frequency dependence of the μGMR at frequencies up to 5.5 GHz. In general, the frequency dependence of the μGMR is weak, but there is a trend to a decrease in the effect with increasing frequency. However, it should be noted that this trend is more related to the measurement technique than to the μGMR.

CoFe/Cu System

Multilayer nanostructures of the CoFe/Cu system are distinguished by high magnetoresistance. The largest value of ~110% was obtained at room temperature in $[Co_{0.95}Fe_{0.05}/Cu]_{120}$ superlattices [81]. Despite lower magnetoresistance, $[Co_{0.9}Fe_{0.1}/Cu]_n$ superlattices are characterized by weak hysteresis and high temperature stability, which is important for use in sensors. For this type of superlattice, the maximum value of the relative magnetoresistance of more than 80% was recently obtained [31].

Measurements of the μGMR effect in the transmission and reflection of microwaves were performed in [59]. In this work, the authors used samples of the spin-valve type, obtained by magnetron sputtering, Ta(10)/NiFe(3)/IrMn(6)/CoFe(t_{CoFe})/Cu(2.5)/CoFe(1)/NiFe(2)/Ta(2), where the thickness of the CoFe t_{CoFe} layer varied from 1.5 to 3.5 nm. In this work, a different definition of the transmission coefficient was used. In [59], following [50], the transmission coefficient d_p was defined as the ratio between the powers of transmitted and incident waves. As a result, instead of (17),
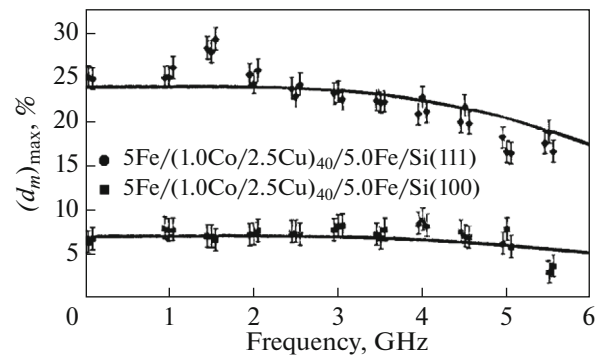
the relationship $d_p \approx 2r$ was obtained. It is easy to check that, for $r \ll 1$, this relationship is equivalent to (17).

The microwave transmission method was used in [82] to study the μGMR effect in $[Co_{0.9}Fe_{0.1}/Cu]_n$ superlattices. Samples of superlattices, the magnetoresistance of which is shown in Fig. 4, were used. The results of microwave measurements are compared with the GMR measurements in Fig. 14. It follows from Fig. 14 that, for the system under consideration, relationship (17) is satisfied approximately, namely, the values of μGMR and GMR are approximately equal and the saturation fields also coincide. Here, the relative change in the transmission coefficient is introduced by analogy with (4a). At present, the ~78% change shown in Fig. 14b are record-high for the μGMR effect.

FeNi/V System

Nanostructures with vanadium layers are interesting for the possibility of regulating the interlayer exchange interaction due to their saturation with hydrogen [83, 84]. Microwave measurements of the transmission coefficient were carried out on $(Fe_{0.82}Ni_{0.18})/V$ superlattices [34, 85]. For the μGMR and GMR effects to be noticeable, the magnetic moments in the adjacent $Fe_{0.82}Ni_{0.18}$ layers must be exactly or approximately antiparallel. It was found in [84] that the GMR effect is observed at a thickness of V layers from 12 to 15 monatomic layers. Antiparallel ordering of magnetic moments is realized in a $(100)MgO/[Fe_{0.82}Ni_{0.18}(1.47)/V(1.77)]_{25}/Pd(6)$ superlattice. Here, the thickness of the vanadium layer is 12 monolayers. Figure 15 shows the field dependences of the GMR and the dependences of the relative change in the transmission coefficient, measured for two orientations of the magnetic field: $H \,/\!/\, H_\sim$ and $H \perp H_\sim$. Microwave measurements were performed at a frequency $f = 37$ GHz. The field dependences of the μGMR and GMR have a similar shape. The magnitude of the μGMR in saturation is slightly higher than
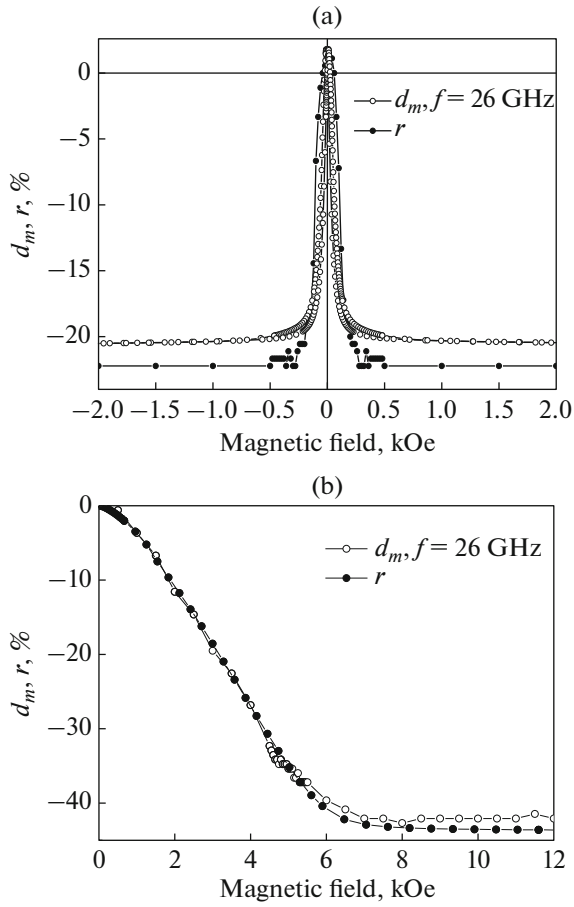
(a)

(b)

Fig. 14. Comparison of the field dependence of the microwave transmission coefficient at a frequency of $f = 26$ GHz and the relative magnetoresistance of the sample: (a) Ta(5)/RuCr(5)/[Co$_{88}$Fe$_{12}$(1.3)/Cu(2.05)]$_8$/Co$_{88}$Fe$_{12}$(1.3)/RuCr(3); (b) Ta(5)/RuCr(5)/[Co$_{88}$Fe$_{12}$(1.5)/Cu(0.95)]$_{24}$/Ta(5).

Fig. 15. The µGMR effect upon microwave transmission through a (Fe$_{0.82}$Ni$_{0.18}$)/V superlattice: comparison between GMR and microwave transmission for two orientations of the magnetic field: **H** // **H**$_\sim$ and **H** $\perp$ **H**$_\sim$.

that of the GMR; nevertheless, the equality $d_m \approx r$ is approximately satisfied.

In addition, the µGMR has been measured in several other systems. In [86], the µGMR was studied in films made of ferromagnetic metal-dielectric composites with compositions Co$_{51.5}$Al$_{19.5}$O$_{29}$, Co$_{50.2}$Ti$_{9.1}$O$_{40.7}$, Co$_{52.3}$Si$_{12.2}$O$_{35.5}$ and (Co$_{0.4}$Fe$_{0.6}$)$_{48}$(MgF)$_{52}$. Microwave measurements were performed at frequencies from 30 to 50 GHz. The results are compared with the data of the magnetorefractive effect. For the first two compositions, strong changes in the microwave transmission coefficient proportional to the GMR are observed. For the other two compositions, the microwave transmission coefficient is independent of the magnetic field. The experimental results are interpreted taking into account the fact that, in the nanocomposite, besides the conduction currents, there are displacement currents, and it is concluded that a giant magnetoimpedance is observed only for such metal-dielec-
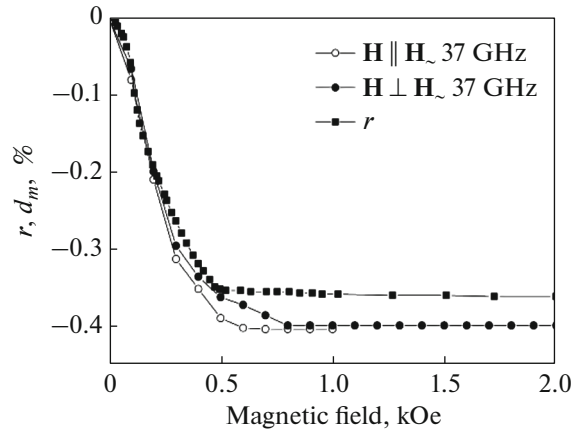
tric nanocomposites in which the content of metal particles exceeds the percolation threshold.

Microwave and magnetic properties of AgPt/Co nanostructures were studied in [87]. For an (Ag + Pt)(5.0)/[(Ag + Pt)(3.0)/Co(0.5)]$_{18}$ (Ag + Pt)(5.0) sample, it was found that the microwave magnetoresistance is the same for **H** // **H**$_\sim$ and **H** $\perp$ **H**$_\sim$ and is of the same order as the negative magnetoresistance in the GMR. In both GMR and µGMR, complete saturation in a magnetic field up to 12 kOe is not achieved.

The transmission coefficient through a [Ni$_{80}$Fe$_{20}$(5.0)/Cu(2.2)/Co(2.0)/Cu(2.2)]$_3$ nanostructure was studied in [10]. The measurements were carried out in the infrared range with a wavelength of 10.6 µm. It was established that the field dependence of the transmission coefficient is similar to the dependence for the GMR, but the changes in the transmission coefficient turned out to be several times smaller than the GMR effect.

Summarizing the results of this section, we come to the conclusion that the one-to-one correspondence of the relative magnetoresistance and the change in the microwave transmission coefficient has been confirmed experimentally more than once for Fe/Cr, Co/Cu, AgPt/Co, (FeNi)/Cu, and (CoFe)/Cu nanostructures. This correspondence is fulfilled both for nanostructures with solid layers and for nanostructures with discontinuities. This correspondence is observed for spin valve nanostructures such as Ta(10)/NiFe(3)/IrMn(6)/CoFe(d_{CoFe})/Cu(2.5)/CoFe(1)/NiFe(2)/Ta(2). According to (17), the quantity d_m does not have a strong frequency dispersion if there is no dispersion of conductivity. The one-to-one correspondence is not observed for metallic nanostructures with discontinuous (cluster-layered) layers of a ferromagnetic metal, for ferromagnetic metal-dielectric nanostructures
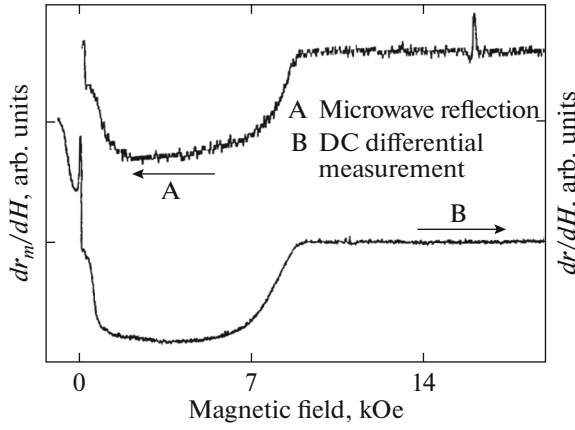
Fig. 16. Dependence of the derivative of the magnetoresistance with respect to the magnetic field and the microwave reflection coefficient measured at a frequency of 70 GHz for a sample of a Fe/Cr superlattice: data from [57].

with a concentration of metal particles below the percolation threshold, and for measurements in the infrared range.

7. MICROWAVE MAGNETORESISTIVE EFFECT IN THE REFLECTION OF MICROWAVES

The μGMR effect in the reflection of microwaves was experimentally observed for the first time in [57], where the coefficient of reflection from a Fe/Cr superlattice sample placed in the cross section of a waveguide but not completely covering the waveguide was measured. Using this technique, it is possible to study the dependence of the reflection coefficient on the magnetic field, to detect the μGMR saturation field, but it is difficult to quantify the μGMR. The measurements in [57] were performed at a frequency of 70 GHz using a modulation technique. The derivatives of the reflection coefficient and electrical resistance with respect to the magnetic field, obtained as a result of measurements, are shown in Fig. 16. There is a similarity of these dependences in a wide range of magnetic fields. An exception is the region around 16 kOe, where the microwave signal has a resonant singularity caused by the FMR.

The study of the μGMR was further developed in [58, 88]. Experiments using the technique in which the superlattice sample completely covers the cross section of the waveguide were conducted. The shape of the field dependence of the reflection coefficient rather than its derivative was determined. Experiments on the joint observation of the μGMR and FMR were carried out, and a simple formula was derived making it possible to calculate the changes in the reflection coefficient from the nanostructure if the relative magnetoresistance is known. Further consideration of the

μGMR effect in the reflection of microwaves will follow [58, 88].

We begin our consideration with formulas (15) for the transmission and reflection coefficients. We will consider these formulas for the limiting case of $d \ll \delta$ that is realized on the decimeter, centimeter, and millimeter waves. Two situations are possible, in which one or another term prevails in the denominator of Eq. (15). The condition $2Z_m\cosh(k_m d) \gg Z\sinh(k_m d)$ corresponds to extremely small nanostructure thicknesses. In this limiting case, the reflection coefficient is

$$R \approx -\frac{Z}{2Z_m}\tanh k_m d, \qquad (21)$$

and, at $d \ll \delta$, the reflection coefficient R is small. If, in the denominator of Eq. (15), the opposite inequality $2Z_m\cosh(k_m d) \ll Z\sinh(k_m d)$ holds, then the transmission and reflection coefficients are expressed as

$$D = \frac{2Z_m}{Z\sinh k_m d}, \quad R = -1 + \frac{2Z_m}{Z}\cosh k_m d. \qquad (22)$$

It can be seen from formulas (22) that the reflection coefficient is close to −1 and its variations are small, since $k_m d \ll 1$. In this limiting case, the coefficients D and R depend on frequency due to the frequency dispersion of the constants and due to the frequency dependence of the impedance of the waveguide, Z. This dependence of Z is weak far from the cutoff frequency of the waveguide, $f_c = \dfrac{c}{2a}$. If the changes in the reflection coefficient are caused only by the magnetoresistance of the nanostructure at $\mu \approx 1$, then, for a thin nanostructure, hyperbolic functions can be expanded in a series. Restricting the expansion to the leading terms, we obtain for the reflection coefficient

$$R = -1 + \frac{2\rho}{Zd}. \qquad (23)$$

For the relative change in the reflection coefficient in a magnetic field, from expression (23), we can obtain

$$r_m = -D(0)[1 - D(0)]r,$$
$$\text{where} \quad D(0) = \frac{2\rho}{Zd\mu(0)}. \qquad (24)$$

Recall that the impedance for a nanostructure sample placed in a rectangular waveguide is calculated by the formula

$$Z = \left(\frac{\mu_0}{\varepsilon_0}\right)^{1/2} \times \left[1 - (\lambda/\lambda_c)^2\right]^{-1/2}, \quad \lambda_c = 2a. \qquad (25)$$
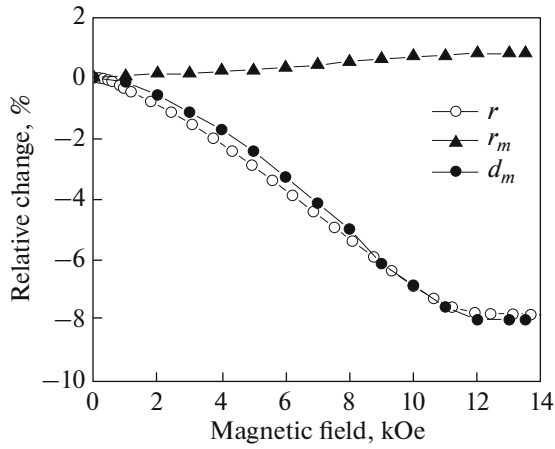
Fig. 17. Microwaves reflection coefficient of a $[(1.8)/Fe(2.8)]_{12}/Cr(7.7)/MgO$ superlattice vs. the magnetic field strength, measured at a frequency of 37 GHz.

Fig. 18. Frequency dependence of the maximum changes in the reflection and transmission coefficients upon magnetization in a field of 12 kOe for a $[Cr(1.3)/Fe(2.9)]_4/Cr(8.2)/MgO$ superlattice.

If measurements are taken in free space, the formula for the impedance takes the form

$$Z = \left(\frac{\mu_0}{\varepsilon_0}\right)^{1/2}. \tag{25a}$$

The results of measuring the field dependences of the GMR and relative changes in the transmission and reflection coefficients at a frequency $f = 37$ GHz for a $[Cr(1.8)/Fe(2.8)]_{12}/Cr(7.7)/MgO$ superlattice are shown in Fig. 17. The equality of the GMR and µGMR is fulfilled with high precision. Variations in the reflection coefficient, in accordance with (24), have a sign opposite to the GMR, a smaller value, and a similar field dependence.

Figure 18 shows the frequency dependence of the maximum changes in the reflection and transmission coefficients for a $[Cr(1.3)/Fe(2.9)]_4/Cr$ (8.2)/MgO superlattice, measured in a field $H = 12$ kOe. It can be seen that the coefficients have only a weak frequency dependence, the changes in the transmission and reflection coefficients have the opposite sign, and the changes in the reflection coefficient are much smaller in magnitude. All these features are consistent with formulas (23) and (24).

A detailed study of the µGMR in the transmission and reflection of electromagnetic waves from Ta(10)/NiFe(3)/IrMn(6)/CoFe(t_{CoFe})/Cu(2.5)/CoFe(1)/NiFe(2)/Ta(2) spin valves was performed in [59], in which the thickness of the CoFe t_{CoFe} layer varied from 1.5 to 3.5 nm. Figure 19 shows the field dependences of the relative changes in the transmission and reflection coefficients, measured at a frequency of 10 GHz, and of GMR for a Ta(10)/NiFe(3)/IrMn(6)/CoFe(3.5)/Cu(2.5)/CoFe(1)/NiFe(2)/Ta(2) nanostructure. Since the transmission and reflection
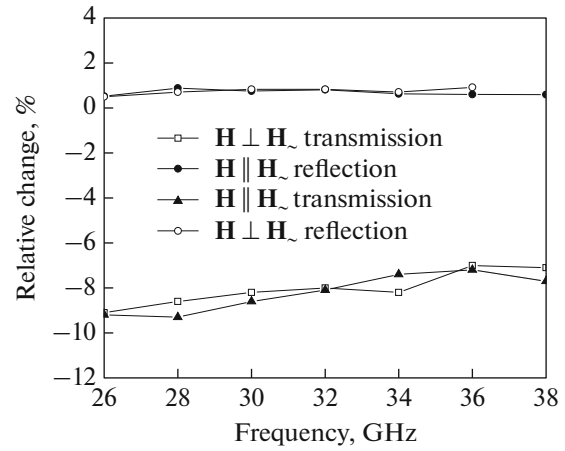
coefficients in this work were introduced in terms of power, we can assert that equality (17) is satisfied in this case as well. In accordance with (24), the reflection coefficient has an opposite sign and a smaller value.

In [59], expressions were obtained making it possible to calculate the relative changes in the coefficients via the changes in the surface resistance of the nanostructure:

$$d_m = \frac{2R_0}{R_0 + 2R_S}r_S, \quad r_m = \frac{-4R_S}{R_0 + 2R_S}r_S, \tag{26}$$

where r_S is the relative change in the surface resistance R_S under the assumption that $R_S \propto \rho$. The value of R_0 is calculated by the formula $R_0 = \omega\mu_0/\beta$, where μ_0 is the permeability of the vacuum and β is the propagation constant in an empty waveguide.
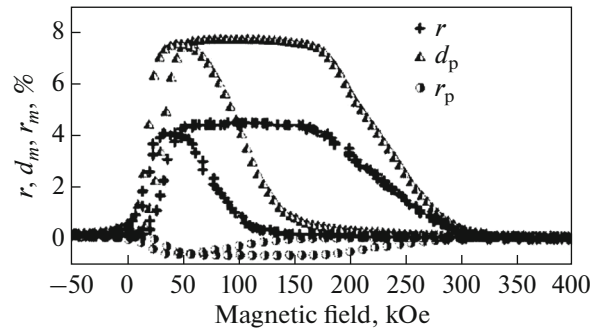

Fig. 19. Relative changes in the transmission and reflection coefficients vs. the magnetic field, measured at a frequency of 10 GHz, and GMR for a Ta(10)/NiFe(3)/IrMn(6)/CoFe(3.5)/Cu(2.5)/CoFe(1)/NiFe(2)/Ta(2) nanostructure: data from [59].
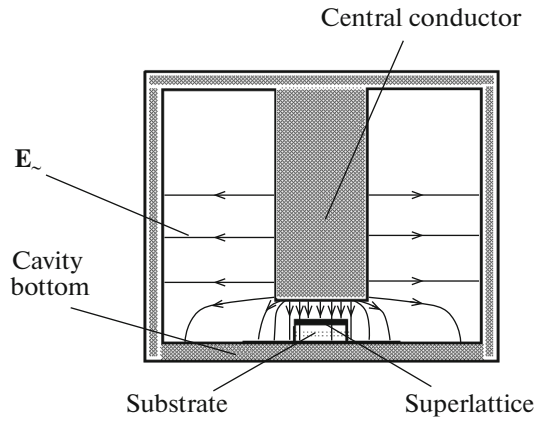
Fig. 20. Superlattice sample in a coaxial resonator.

8. MICROWAVE MAGNETORESISTIVE EFFECT WHEN THE CURRENT IS PERPENDICULAR TO THE NANOSTRUCTURE LAYERS PLANE

It was noted in Section 2 that there are two variants of GMR measurements, in which the electric current flows in the plane of the nanostructure (the current-in-plane geometry, CIP) and perpendicular to the plane (the current-perpendicular-to-plane geometry, CPP). The latter option has the advantage that the relative magnetoresistance is higher. However, the implementation of the experiment in the CPP geometry encounters certain difficulties. One of the main difficulties is the extremely low resistance of the sample, since the typical thickness of the metal of the nanostructure usually does not exceed 300 nm. Methods for making such measurements using modulation techniques and bridge circuits have been developed. However, the μGMR can be measured in the CPP geometry by a simpler method at frequencies of hundreds of megahertz [89–91]. The schematic diagram of the experiment to study the current flow perpendicular to the plane of the nanostructure layers (CPP) at high frequencies is shown in Fig. 20.

The electric field in the coaxial resonator is concentrated between the end face of the central conductor and the bottom of the resonator, and the lines of the high-frequency magnetic field envelop the central conductor. The superlattice sample is placed in the region of a strong electric field. The magnetoresistance of the sample significantly changes the loss in the resonator as the magnetic field changes; therefore, the absolute value of the transmission coefficient also changes. The absolute value of the transmission coefficient of the resonator that is included as a feedthrough element, is determined as follows [92]:

$$D = \frac{2Q_L^2}{Q_1 Q_2} \frac{1}{1 + Q_L^2 (\Delta\omega/\omega_0)^2}. \tag{27}$$

Here, Q_L is the loaded Q-factor of the resonator with the sample, and Q_1 and Q_2 are the Q-factors introduced by the coupling of the resonator with two transmission lines: to the oscillator and to the measuring detector. In formula (27), $\Delta\omega$ is the detuning from the resonant frequency ω_0. At the resonant frequency, the transmission coefficient is

$$D = \frac{4Q_L^2}{Q_1 Q_2}, \quad \omega = \omega_0. \tag{28}$$

On the right-hand side of formula (28), only the loaded Q-factor $Q_L = Q_L(H)$ changes in an external magnetic field. In [90, 91], the intrinsic Q-factor of the resonator with a sample was calculated taking into account the power loss $P_{\text{Loss}} = 1/2\int|H_t|^2 R_S \, dS$, where the surface resistance R_S is the resistance of a unit-area conductor with a length equal to the thickness d of the superlattice metal layer and having an electrical resistivity ρ_{eff}: $R_S = \rho_{\text{eff}} d$. We can now find the relationship between the transmission coefficient in a magnetic field, $D(H)$, and without a field, $D(0)$:

$$\xi = \frac{\int_{S_S} |H_t|^2 R_S dS}{\int_S |H_t|^2 R_S dS}, \quad 0 < \xi < 1,$$

$$\frac{D(H)}{D(0)} = \left[1 + \xi \frac{Q_L(0)}{Q_0} \frac{R_S(H) - R_S(0)}{R_S(0)} \right]^{-2}. \tag{29}$$

In formula (29), a parameter ξ is introduced that takes into account the fraction of the loss in the sample due to all intrinsic losses of the resonator, where H_t is the tangent component of the high-frequency magnetic field on the surface of the sample, S_S, and on the surface of the resonator, S. If $|\xi(Q_L(0)/Q_0)r| \ll 1$, then the relative change in the absolute value of the transmission coefficient is expressed by the simple formula

$$d_m = -2\xi \frac{Q_L(0)}{Q_0} r. \tag{30}$$

If the loss in the resonator is almost entirely determined by the loss in the sample, then $\xi \approx 1$ and (30) transforms into a simple formula given in [89, 90]:

$$d_m = -2r. \tag{31}$$

Thus, the change in the transmission coefficient through the resonator with a sample is equal to the doubled relative change in the resistance taken with the opposite sign.

In [91], using Maxwell equation for the divergence of the electric field and the kinetic equation together with the boundary conditions written for a metal plate, the expressions for the distribution of the high-frequency electric field $E_\sim$ and current density $j_\sim$ over the

depth of the superlattice (along the z-coordinate) were obtained:

$$E_\sim(z) = \left(\frac{\omega_p Z_D}{v_F}\right)^2 e^{-z/Z_D} E_\sim(0) + \left[1 - \left(\frac{\omega_p Z_D}{v_F}\right)^2\right] E_\sim(0),$$

$$j_\sim(z) = \frac{i\omega}{4\pi}\left(\frac{\omega_p Z_D}{v_F}\right)^2 (e^{-z/Z_D} - 1) E_\sim(0),$$

$$Z_D = \frac{v_F}{\sqrt{\omega_p^2 - i\omega(v - i\omega)}},$$

where $\omega_p = (4\pi n e^2/m)^{1/2}$ is the plasma frequency, n and m are the density and effective mass of the current carriers, v_F is the Fermi velocity, $E_\sim(0)$ is the electric field on the sample surface, Z_D is the screening parameter, and v is the effective collision frequency. At $\omega \ll \omega_p$, $v \ll \omega_p$,

$$Z_D \approx r_D\left(1 + \frac{\omega^2}{\omega_p^2} + i\frac{\omega v}{\omega_p^2}\right), \quad r_D = \frac{v_F}{\omega_p},$$

r_D is the Debye screening length. It can be seen from the above formulas that the field $E_\sim$ and the current $j_\sim$ consist of two components. One is due to the dynamic analogue of the electrostatic screening effect; it decays exponentially at a depth of the order of the screening length. The second one is the penetrating component that penetrates the entire cross section of the sample. In particular, inside the metal, there is an electric field

$$\left|E_\sim(z \to \infty)\right| \cong E_\sim(0)\frac{2\omega v}{\omega_p^2}.$$

This penetrating component exists only if the thickness of the metal layer is significantly smaller than the skin depth. The power of electromagnetic oscillations in the sample is calculated as

$$P = S_S\int_{V_S} j_\sim{}^* E_\sim dV,$$

where the integration is performed over the sample volume. The loss in the sample is described by the real part of P:

$$\begin{aligned}P_{\text{Loss}} &= \operatorname{Re} P = \frac{\omega^2 v}{2\pi\omega_p^2} dS_S E_\sim^2(0) \\ &= \frac{\omega^2 R_S}{8\pi^2} S_S E_\sim^2(0).\end{aligned} \tag{32}$$

According to (32), the power loss is directly proportional to the surface resistance R_S, in full accordance with (30).

An experimental validation of formula (30) was performed in [52, 89, 90]. The measurements in [52] were performed on three superlattices: (1) $[Fe(2.1)/Cr(1.0)]_{12}$, (2) $[Fe(1.4)/Cr(0.9)]_{30}$, and (3) $[Fe(2.1)/Cr(1.7)]_{12}$. High-frequency measurements were performed at 779 MHz. It can be seen
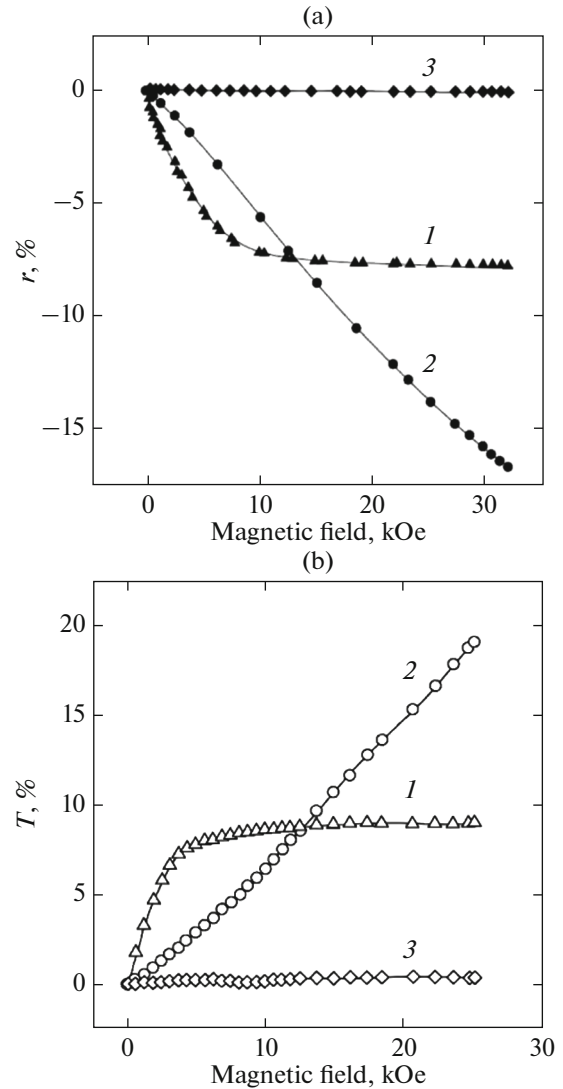
Fig. 21. (a) Relative magnetoresistance and (b) relative change in the transmission coefficient in the CPP geometry vs. the magnetic field for three Fe/Cr superlattice samples.

from Fig. 21a that these samples have different types and magnitudes of the GMR. Figure 21b shows the relative change in the transmission coefficient of the resonator with a sample. It is seen that the high-frequency changes have the sign opposite to the GMR. The type of dependence of the µGMR for each sample is similar to that of the GMR. It can be seen that high-frequency changes are approximately 1.2−1.4 times greater in absolute value than the GMR.

In conclusion of this section, we note that the CPP geometry of the high-frequency currents can be realized on traveling waves if a nanostructure with a metal thickness smaller than the skin depth is placed along the waveguide axis in parallel to its larger wall [71].

9. MICROWAVE MAGNETORESISTIVE EFFECT IN A WIDE FREQUENCY RANGE

In this section, we will analyze a formula for the coefficient of transmission of electromagnetic waves through a thin metal plate (15) for a wide range of frequencies. We consider the following special cases: (1) microwave frequencies, (2) low frequencies and/or very thin films, and (3) frequencies in the upper part of the millimeter-wavelength range. The µGMR will be studied for films and nanostructures with both high and moderate conductivity. The presentation will follow [79, 93].

Let us analyze the penetration of the electromagnetic field through a superlattice. The transmission coefficient D depends on the ratio of the impedances of the superlattice, Z_m, and the ambient space, Z, and the ratio of the total thickness of the metal in the superlattice, d, and the skin depth δ. If the sample is placed in a waveguide, then the impedance is calculated by formula (25), and, if the experiment is carried out in free space, then the impedance is calculated by formula (25a).

Consider the limiting case of formula (15), when $d \ll \delta$. The low-frequency interval (radio and lower frequencies) corresponds to the condition $2Z_m\cosh(k_m d) \gg Z\sinh(k_m d)$ in the denominator of (15). In this case, using the condition $d \ll \delta$, we obtain

$$|D| \approx 1 - [1/3\,(d/d)^4].\tag{33}$$

It is clear that, in this case, the absolute value of the transmission coefficient is close to unity. Hence, it is easy to obtain an expression for the relative change:

$$d_m = -\frac{1}{12}d^4\omega^2\mu_0^2\left(\frac{\mu^2(H)}{\rho^2(H)} - \frac{\mu^2(0)}{\rho^2(0)}\right).$$

The quantity d_m is small due to the inequality $d \ll \delta$. In saturation fields, $\mu(H) \approx 1$; with a small magnetoresistance $\rho(H) \approx \rho(0)$ and a large initial permeability $\mu \gg 1$, we have

$$d_m \approx \frac{d^4\mu^2(0)\mu_0^2}{12\rho^2(0)}\omega^2.\tag{34}$$

Changes in the transmission coefficient at radio frequencies and $\mu(0) \gg 1$ can be caused by the change in the permeability. They are small, $d_m \ll 1$, positive, and, in the absence of frequency dispersion of the material constants, proportional to ω^2.

Now let us consider the range of the centimeter and millimeter waves. If, in the denominator of (15), $2Z_m\cosh(k_m d) \ll Z\sinh(k_m d)$, then the transmission coefficient is expressed by formula (16):

$$D = \frac{2Z_m}{Z\sinh k_m d}.\tag{35}$$

For a thin nanostructure with $d \ll \delta$ and $\mu(H) \approx 1$, from (35), we obtain

$$D = \frac{2\rho}{Zd}.\tag{36}$$

In this limiting case, the transmission coefficient is real if the impedance ρ is real. It depends on the frequency through the impedance Z, and this dependence is weak far from the cutoff frequency of the waveguide, $f_c = \dfrac{c}{2a}$. For the experiments in free space, if the impedance is expressed by formula (25a), this source of dispersion is totally absent. Formula (35) implies one-to-one correspondence (17) between the magnetoresistive effect measured at direct current and the transmission coefficient, if $\mu \approx 1$.

Now let us consider a wider frequency range, including those frequencies at which $2Z_m\cosh(k_m d) \sim Z\sinh(k_m d)$. We will perform numerical calculations of the dependences of the transmission and reflection coefficients on the magnetic field by formulas (15), assuming the conductivity of the nanostructure in zero field $\sigma(0) = 1.26 \times 10^6$ S/m and the magnetoresistance shown in Fig. 7a. The calculations were performed for several values of the nanostructure thickness d from 0.5 to 50 nm. The results of calculating the coefficients are shown in Fig. 7 [93]. For sufficiently large thicknesses, the magnitude of the changes in the transmission coefficient d_m is close to the relative magnetoresistance r and the shape of the field dependence of d_m is similar to the field dependence of the magnetoresistance. The opposite limiting case, described by formula (33), for this high value of the nanostructure conductivity is not achieved even at a very small nanostructure thickness of 0.5 nm. It should be noted that the maximum changes in the reflection coefficient r_m are achieved at an intermediate value of the thickness, $d = 3$ nm. Figure 7c shows the calculated dependence of the changes in d_m and r_m in a field of 12 kOe, i.e., at magnetic saturation, as a function of the nanostructure's thickness. It can be seen that, in the entire range of the thickness d, the relative change in the coefficient is negative and monotonically increases in absolute value with increasing d. At large thicknesses, the microwave variation in d_m tends to the relative magnetoresistance r. In contrast, the relative change in the microwave reflection coefficient has a maximum; with a further increase in the thickness of the nanostructure, it decreases and tends to the value prescribed by formula (24).

Now let us consider the calculation results for a nanostructure with a low conductivity, $\sigma(0) = 1 \times 10^3$ S/m. This value of conductivity can belong, e.g., to a nanostructure containing a semiconductor or a semimetal. The rest of the parameters of the nanostructure are the same as in the above case. We assume that the magnetoresistance of the nanostructure is as shown in Fig. 7a. In this case, we consider a wider range of nanostructure

thicknesses from 0.5 to 300 nm. The results of calculating the transmission and reflection coefficients are shown in Fig. 22a.

The shape of the field changes in the dependences of the transmission coefficient is similar to the shape of the dependence of the magnetoresistance measured at direct current, but the changes in the transmission coefficient d_m is much smaller than the relative magnetoresistance. Hence, we can conclude that, in the entire reasonable range of nanostructure thicknesses up to 300 nm, at millimeter (and even more so, centimeter) wavelengths, the limiting case of the one-to-one correspondence $d_m = r$ for nanostructures with a low conductivity $\sigma(0) = 1 \times 10^3$ S/m is not achieved. Figure 22b shows the dependences of the transmission and reflection coefficients in a field $H = 12$ kOe on the thickness of the nanostructure. These dependences are noticeably different from the dependences shown in Fig. 7c. The changes in the transmission coefficient are many times smaller than the magnetoresistance, and the thickness dependence in the considered range of parameters is close to linear. The thickness dependence of the reflection coefficient has no maximum.

In this section, we considered the microwave giant magnetoresistive effect in magnetic metallic nanostructures in a wide frequency range. Numerical calculations have been carried out to refine the frequency characteristics of this effect. From the general expressions for the transmission and reflection coefficients for a metal plate with a magnetoresistive effect, it follows that there are two limiting cases with very different characteristics of the microwave giant magnetoresistive effect. The first limiting case cannot be realized in metallic nanostructures with a thickness greater than 0.5 nm. The second limiting case is realized at frequencies of the centimeter- and millimeter-wavelength ranges for metallic nanostructures with a thickness of 0.5 to 200 nm. On the contrary, for nanostructures with a low conductivity of ~10^3 S/m, the second limiting case and the one-to-one correspondence of the μGMR and GMR at microwave frequencies are not realized.

10. FERROMAGNETIC RESONANCE AND THE MICROWAVE MAGNETORESISTIVE EFFECT

In this section, we will consider the joint manifestation of the ferromagnetic resonance and the microwave giant magnetoresistive effect in metallic nanostructures. We will describe the specifics of the manifestation of the FMR in the transmission through nanostructures of different types. The FMR spectrum in nanostructures will be considered and information on the interlayer exchange constants will be obtained from it. The state of the art FMR studies in films, prior to the discovery of the GMR effect, are listed in the review [94]. Damping in a magnetic system in thin-
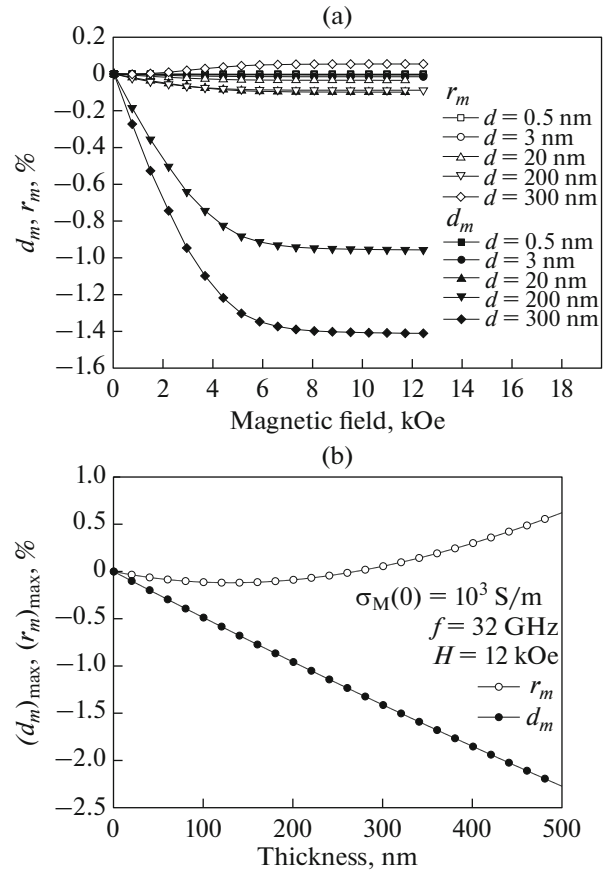

Fig. 22. (a) Field dependences of the transmission and reflection coefficients of a nanostructure with a conductivity $\sigma(0) = 1 \times 10^3$ S/m at a frequency $f = 32$ GHz, calculated for several thicknesses of the nanostructure and (b) relative changes in a field of 12 kOe vs. the thickness of the nanostructure.

film ferromagnets was studied in [95]. In addition to measurements in standard magnetic resonance spectrometers [44], other experimental methods have been developed [48, 96]. We will restrict our consideration to works that use the microwave transmission technique. Of considerable interest is the study of multilayer nanostructures by the FMR method. In particular, from the FMR spectrum, it is possible to obtain information on the interlayer exchange interaction [37, 38, 97].

In [54, 64, 76], the transmission method was used to study the μGMR and FMR phenomena in Fe/Cr nanostructures of different types: superlattices with parallel, antiparallel, and noncollinear ordering of the magnetic moments of adjacent layers, cluster-layered nanostructures, and thin Fe and permalloy films. Let us first consider the results obtained on Fe/Cr superlattices with a low saturation field H_s, for which the FMR conditions are realized after the sample reaches magnetic saturation. Figure 8 shows the results of measurements performed on this type of
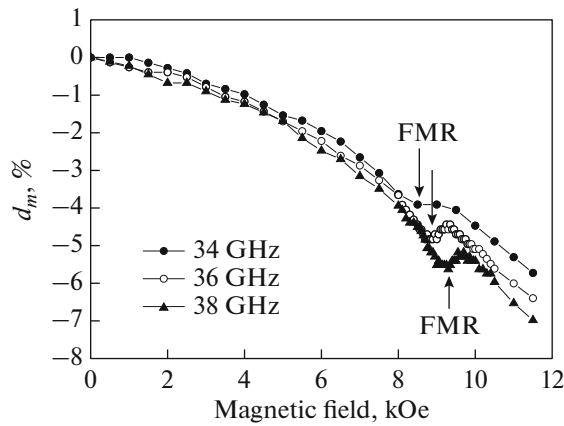
Fig. 23. Microwave transmission coefficient vs. the magnetic field for a Cr(1.0)/[Fe(1.06)/Cr(1.1)]$_{30}$/Cr(8)/MgO superlattice.

[Cr(1.8)/Fe(2.8)]$_{12}$/Cr(7.7)/MgO superlattice at different frequencies for **H ⊥ H**$_~$. It is seen that the field dependence of variations in the transmission coefficient d_m in a certain narrow range of fields has a resonant singularity (minimum). It should be noted that the nonresonant part of the dependence $d_m(H)$ was approximately the same in the entire frequency range under study and is very similar to the field dependence of the magnetoresistance measured at direct current. The resonant contribution was observed at frequencies exceeding 30 GHz, and the field of the minimum transmission coefficient increases with increasing frequency. For the case of **H // H**$_~$, the minimum associated with the FMR was not observed.

On a [Cr(1.1)/Fe(0.9)]$_{40}$/Cr(8.5)/MgO superlattice with thin layers and a high saturation field, the absorption minimum due to the FMR was observed with **H ⊥ H**$_~$ in a field weaker than the magnetic saturation field of the sample. Figure 9a shows the dependences $d_m(H)$ determined at a frequency of 36 GHz for **H ⊥ H**$_~$ and **H // H**$_~$, as well as the field dependence of the magnetoresistance, $r(H)$, measured at a direct current. It turned out that the resonance amplitude at $f = 36$ GHz for this sample is much lower than that for a [Cr(1.8)/Fe(2.8)]$_{12}$/Cr(7.7)/MgO sample magnetized to saturation. Microwave transmission was also studied on a [Cr(1.1)/Fe(0.4)]$_{50}$/Cr(8.5)/MgO cluster-layered nanostructure. The results are shown in Fig. 9b. No resonant changes were observed in the cluster-layered Fe/Cr nanostructure. This is consistent with the magnetization measurement results. The absence of a hysteresis loop and the absence of a resonant contribution to microwave transmission indicate that the Fe layers are not continuous, but consist of individual Fe clusters (islands).

If the magnetic characteristics of the superlattice are such that the resonance falls on the magnetically unsaturated state of the superlattice, then the FMR spectrum will depend on the interlayer exchange constants. It will be explained below how these constants can be determined from the FMR spectrum. Figure 23 shows the dependences of the coefficient of transmission through a Cr(1nm)/[Fe(1.06)/Cr(1.1)]$_{30}$/Cr(8)/MgO superlattice, measured at several frequencies of the millimeter-wavelength range. From the resonant field, the spectrum can be reconstructed.

The FMR spectra were studied in [35, 36, 98−100]. In [35, 36], the spectra were calculated taking into account the interlayer exchange interaction, including inhomogeneous modes, and the spectra were obtained experimentally for several Fe/Cr superlattices. One of the goals of these works was to obtain the numerical constants in the biquadratic approximation of the interlayer exchange interaction.

The spectra of the homogeneous acoustic vibration mode are important for us, since resonances belonging to this mode are observed experimentally by the transmission method. The equations of the frequency spectrum of the acoustic mode are different for the saturated and unsaturated states:

$$\omega = \gamma M[2C(2C + K_{\text{eff}})]^{1/2}, \quad H \leq H_s, \quad (37)$$

$$\omega = \gamma[H(H + K_{\text{eff}}M_s)]^{1/2}, \quad H > H_s. \quad (38)$$

The quantity C is expressed via the constants A and B from the expression for the magnetization curve (2) or via the exchange constants J_1 and J_2:

$$C = \frac{A + BM^2}{2} = \frac{2}{dM_s^2}\left[J_1 - 2J_2\left(1 - 2\frac{M^2}{M_s^2}\right)\right]. \quad (39)$$

In formulas (37) and (39), the magnetization M can be taken from a measured magnetization curve or from its approximation (2). In numerical calculations of the spectrum, we neglect the effect of uniaxial anisotropy and set $K_{\text{eff}} = 4\pi$. The possibility of such a simplification for Fe/Cr superlattices follows from the data of [36]. The calculated spectra were constructed under the assumption of a uniform precession of magnetic moments in all layers and in all parts of the sample.

Figure 24 shows the FMR spectra of four samples of Fe/Cr superlattices presented in Table 1. Calculations were performed using formulas (37) and (38). The magnetization of the superlattice is taken from the measured magnetization curve, and the exchange constants J_1 and J_2 are taken from Table 1. It can be concluded from Fig. 24 that the calculated spectra are in good agreement with the experimental ones. Therefore, the interlayer exchange constants obtained from the analysis of the magnetization curves are in good agreement with the corresponding values obtained from the FMR spectra.

With increasing frequency, the resonance field increases; as a rule, the resonance amplitude also increases (see Fig. 25). The effect of the wave frequency and the magnetization of the film can be ana-
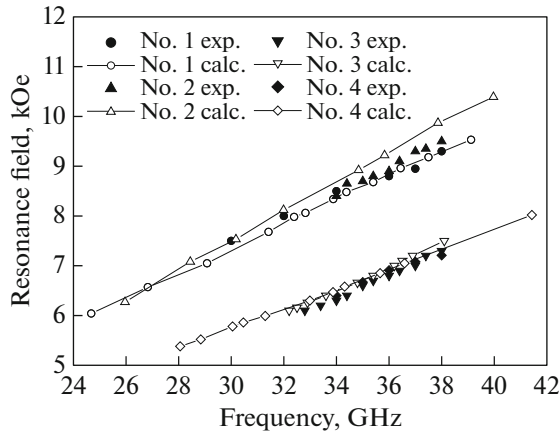
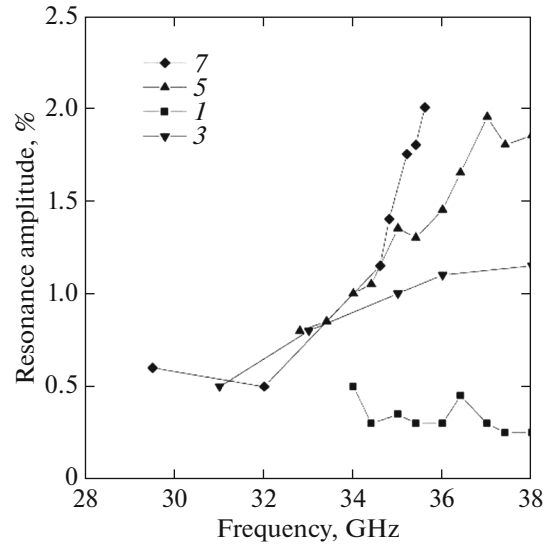**Fig. 24.** Measured and calculated FMR spectra for four Fe/Cr superlattices.

Fig. 25. Frequency dependence of the FMR amplitude upon transmission for several Fe/Cr superlattices: (*1*) $[Cr(11Å)/Fe(9Å)]_{40}/Cr(85Å)/MgO$; (*3*) $[Cr(11Å)/Fe(16Å)]_{30}/Cr(83Å)/MgO$; (*5*) $[Cr(12Å)/Fe(23Å)]_{16}/Cr(77Å)/MgO$; and (*7*) $[Cr(18Å)/Fe(28Å)]_{12}/Cr(77Å)/MgO$.

lyzed based on an approximate formula obtained for a thin ferromagnetic metal film in the case of the normal skin effect [101]:

$$d_{max} \sim \frac{-\omega G}{(\omega - \omega_r)^2 + \left(\frac{\omega G}{\gamma M_s}\right)^2}, \qquad (40)$$

where ω_r is the resonant frequency, $G = \alpha \gamma M_s$ is the Gilbert constant, and d_{max} is the amplitude of changes in the transmission coefficient at the resonance. From (40), it follows that, at the resonance, $d_{max} \sim \gamma^2 M_s^2 / \omega G$, i.e., with increasing magnetization, the resonance amplitude increases. The frequency dependence of the resonance amplitude from (40) differs from that shown in Fig. 25. The term $\left(\omega G / \gamma M_s\right)^2$ in the denominator determines the width of the resonance line. In (40), the width is determined only by the loss in the magnetic system. According to [102, 103], there are several sources of magnetic loss, the ratio between which can vary depending on the film material and temperature. In addition, the imperfection of the crystal structure of the film also contributes to the width of the resonance line. To take into account various contributions to the width of the magnetic resonance line more accurately, its frequency dependence was approximated by a linear function [102, 103]:

$$\Delta H(\omega) = \Delta H(0) + \frac{\omega G}{\gamma^2 M_s}, \qquad (41)$$

where $\Delta H(\omega)$ the linewidth at the frequency ω, and $\Delta H(0)$ is the change in the linewidth due to the imperfection of the structure. A detailed theoretical analysis carried out in [104] with allowance for the exchange interaction and the roughness of the film boundaries has shown that the frequency dependence of the linewidth is nonlinear, which was experimen-

tally confirmed in [95]. However, approximation (41) can be used in a limited frequency range. If we take into account formula (41) in the denominator of (40), then it turns out that the resonance amplitude increases linearly with frequency, which is approximately confirmed experimentally in Fig. 25.

Let us now discuss the orientation of the constant magnetic field required to observe the FMR line in the transmission of microwaves [34]. Figure 26 shows the dependences of the transmission coefficient through a $[Fe_{0.82}Ni_{0.18}(1.03)/V(1.9)]_{100}/Pd(6)$ superlattice, measured for two orientations of the constant magnetic field: $\mathbf{H} \perp \mathbf{H}_\sim$ and $\mathbf{H} // \mathbf{H}_\sim$, at two frequencies: $f = 33$ and 37.5 GHz. The FMR line is clearly observed for $\mathbf{H} \perp \mathbf{H}_\sim$. For the other orientation of the magnetic field, $\mathbf{H} // \mathbf{H}_\sim$, the FMR either is completely absent, as in Fig. 26a, or changes very weakly (Fig. 26b). This picture is consistent with the concept of the effective dynamic permeability [65]. For $\mathbf{H} \perp \mathbf{H}_\sim$, the effective permeability is combined from the components of the dynamic permeability tensor, as shown in formula (8) that includes components that resonantly depend on the frequency and on an external magnetic field. In contrast, for $\mathbf{H} // \mathbf{H}_\sim$, the effective permeability is determined by the susceptibility component (8c) that does not have a resonance singularity. Nevertheless, the dependence measured at a frequency of 37.5 GHz, in Fig. 26, exhibits weak resonant variation for $\mathbf{H} // \mathbf{H}_\sim$. These variations were related both to the presence of spin-wave resonance in this sample at $f = 36$ GHz and to the difference of the dynamic magnetic susceptibility from the Polder form (18).
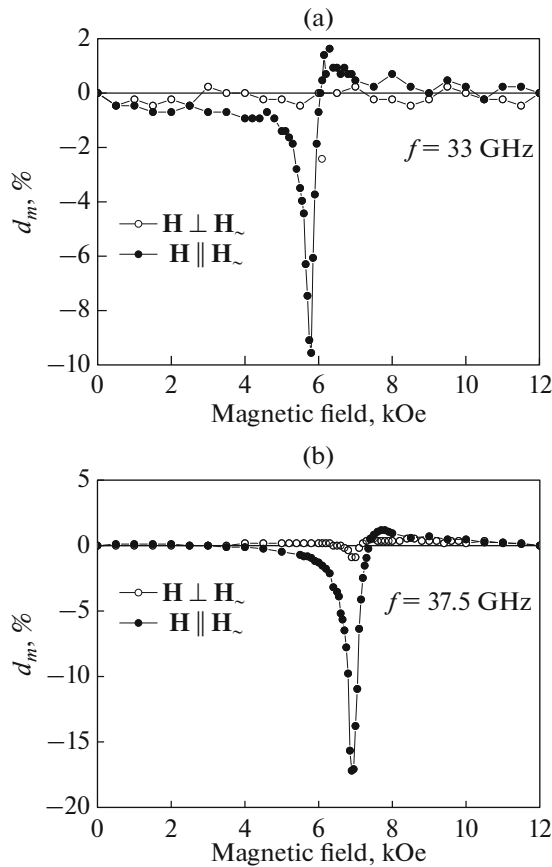
Fig. 26. Comparison of the dependence of the transmission coefficient on the magnetic fi eld for two orientations of the constant magnetic field: (filled symbols) **H ⊥ H₋** and (empty symbols) **H // H₋**. Frequencies f = (a) 33 and (b) 37.5 GHz.

A detailed study of the FMR spectrum was carried out in [85] for three (FeNi)/V superlattices: (1) $(100)\text{MgO}/[\text{Fe}_{0.82}\text{Ni}_{0.18}(0.6)/\text{V}(1.0)]/_{100}/\text{Pd}(6)$, (2) $(100)\text{MgO}/[\text{Fe}_{0.82}\text{Ni}_{0.18}(1.47)/\text{V}(1.77)]_{25}/\text{Pd}(6)$, and (3) $(100)\text{MgO}/[\text{Fe}_{0.82}\text{Ni}_{0.18}(1.47)/\text{V}(0.89)]_{25}/\text{Pd}(6)$. Among them, sample 2 has an antiparallel ordering of the magnetic moments of adjacent layers and the other two samples have parallel ordering.

Figure 27 shows the measured FMR spectra in these superlattices, as well as the spectrum calculated by formula (38) for sample 2. The experimental spectrum for sample 2 is discontinuous, since, in the range of frequencies about 36 GHz, in addition to the FMR, a spin-wave resonance is also observed. The difference between the calculated and measured spectra is noteworthy. This difference is explained in [85] by the presence of "magnetically dead" Fe layers at the interfaces in Fe/V and (FeNi)/V superlattices. Fe atoms in these layers have a much lower magnetic moment [10]. An estimate of the thickness of these layers showed [85] that the thickness of the magnetically dead layers is 1−1.5 Fe monolayers.
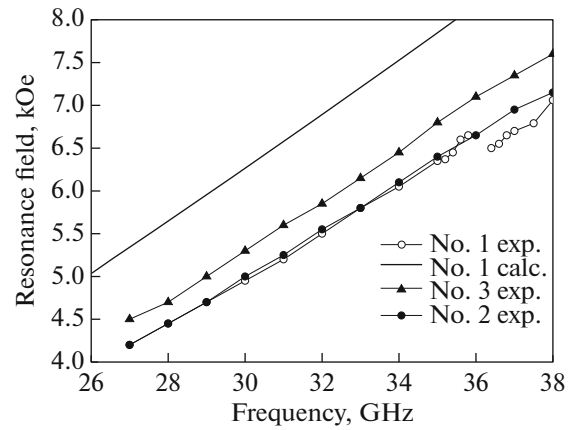

Fig. 27. FMR spectra in $(\text{Fe}_{0.82}\text{Ni}_{0.18})_n/\text{V}_m$ (001) superlattices.

11. SPIN-WAVE RESONANCE UPON THE TRANSMISSION OF MICROWAVES

In this section, we will discuss the observation of the spin-wave resonance (SWR) upon the transmission of electromagnetic waves through metal nanostructures, consider the specificities of the SWR in a magnetic field lying in the plane of the nanostructure, find the conditions for observing spin-wave resonance, and calculate the SWR spectrum.

Spin-wave resonance is achieved when the spin wavelength is equal to or multiple of the characteristic size of a metal object, e.g., the thickness of the film. When a wave passes through a thin film, SWR is observed as a series of peaks (maxima) in the transmission coefficient in the field or frequency dependence of the coefficient [105]. As a rule, to observe SWR, the geometry of the experiment is chosen so that the constant magnetic field is perpendicular to the film plane [106, 107]. The observation of spin-wave resonances in metallic films and nanostructures is hampered by the strong damping of spin waves in metals. However, there are ways to compensate the loss due to the spin-orbit torque effect [108, 109]. The theory of SWR is presented, in particular, in [110]. A theoretical description of the propagation of spin waves in films and nanostructures should take into account the magnetic-dipole and exchange interactions, boundary conditions for spins at boundaries, and magnetic irregularities [65, 111−114]. An investigation of the SWR in a magnetic field parallel to the film plane was performed in [115].

An experimental study of the SWR in a $(100)\text{MgO}/[\text{Fe}_{0.82}\text{Ni}_{0.18}(1.47)/\text{V}(1.77)]_{25}/\text{Pd}(6)$ superlattice was performed in [34]. The field dependences of the transmission and reflection coefficients at frequencies about 36 GHz are shown in Fig. 28. The presence of the SWR is clearly seen in Fig. 28a, in
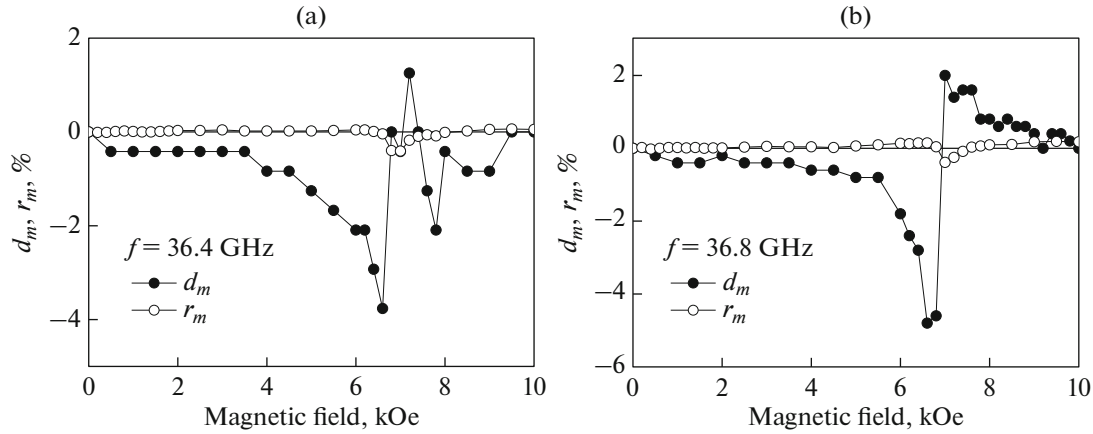
Fig. 28. Ferromagnetic and spin-wave resonances and µGMR upon microwave transmission, d_m, and reflection, r_m, for a (100)MgO/[Fe$_{0.82}$Ni$_{0.18}$(1.47)/V(1.77)]$_{25}$/Pd(6) superlattice, measured at different frequencies about 36 GHz: $f =$ (a) 36.4 and (b) 36.8 GHz.

which there are two resonant lines, and in Fig. 28b, where the resonance line is broadened.

Let us conduct a theoretical discussion of the SWR resonances upon the transmission of microwaves. The fundamentals of the theory were laid out in [116], where the dispersion relation for spin waves in a ferromagnetic metal was obtained and solved. The boundary conditions for spins at the metal boundary were also taken into account [117]. The presentation of this problem follows [34] using the results of [118, 119].

The multilayer nanostructure is replaced by a homogeneous plate with effective conductivity and permeability. The theoretical description starts with Maxwell equations for curls and the Landau−Lifshitz−Gilbert equation:

$$\mathrm{curl}\mathbf{E} = -\frac{1}{c}\frac{\partial}{\partial t}(\mathbf{H} + 4\pi\mathbf{M}); \quad \mathrm{curl}\mathbf{H} = \frac{4\pi\sigma}{c}\mathbf{E}; \quad (42)$$

$$\frac{1}{\gamma}\frac{\partial \mathbf{M}}{\partial t} = \mathbf{M} \times \left[\mathbf{H} + \left(\frac{2A}{M_s^2}\right)\nabla^2\mathbf{M} - \left(\frac{G}{\gamma M_s^2}\right)\mathbf{M}\times\mathbf{H}\right], \quad (43)$$

where $\mathbf{M}$ is the total magnetization vector, σ is the conductivity of the metal, c is the speed of light, A is the exchange parameter, M_s is the saturation magnetization, $\gamma = g|e|/2mc$ is the gyromagnetic ratio, g is the spectroscopic splitting factor, e and m are the charge and mass of the electron, and G is the Gilbert damping constant in the magnetic system. The system of equations (42), (43) is linearized, which results in the dispersion relation

$$K^6 - C_1K^4 + C_2K^2 - C_3 = 0, \quad (44)$$

from which the wavenumbers of the eigenwaves in the metal are found. There are three solutions of Eq. (44): K_1, K_2, and K_3. These solutions correspond to the wavenumbers k_n that are related to Larmor and anti-Larmor spin waves and an electromagnetic-like spin wave.

To find the wave amplitudes, system (42) and (43) must be supplemented with boundary conditions for fields and spins at the boundaries of the media: on two sides of the metal plate and the dielectric plate (substrate). This results in a system of linear equations that can be solved with respect to the amplitudes of the spin eigenwaves in the ferromagnetic plate. The amplitude and polarization of the fields and magnetization inside and at the boundaries of the ferromagnetic plate is obtained by summation taking into account the phases of eigenwaves.

The calculations were performed for a plate with the following parameters. The effective conductivity for this nanostructure was determined experimentally by the method described in [69] and was $\sigma = 2 \times 10^7$ S/m. The magnetization of the Fe$_{0.82}$Ni$_{0.18}$ layers was taken to be $M_s = 1285$ G, based on the coincidence of the calculated and measured FMR fields and took into account magnetic measurements, the constant $\alpha = 0.0085$ is determined from the FMR linewidth, and the exchange constant $A = 5 \times 10^{-6}$ erg/cm is typical of Fe-Ni alloys [65]. The thickness of the metal in the nanostructure (plate thickness) was chosen equal to $d = 290$ nm, which is close to the thickness of the (100)MgO/[Fe$_{0.82}$Ni$_{0.18}$(1.47)/V(1.77)]$_{25}$/Pd(6) nanostructure under study. The parameters of the dielectric substrate were as follows: a thickness $d_s = 0.5$ mm and a permittivity $\varepsilon_s = 8.5$. The calculation results at several frequencies are presented in Fig. 29.

The strongest minimum of the transmission coefficient, located on the right in each graph in Fig. 29, is caused by the microwave absorption under conditions of the resonance of the homogeneous FMR mode. The singularities on the left of the FMR peak are caused by the SWR. They are caused by wave interference over the depth of the plate. Depending on the phase relations, these changes can give singularities of
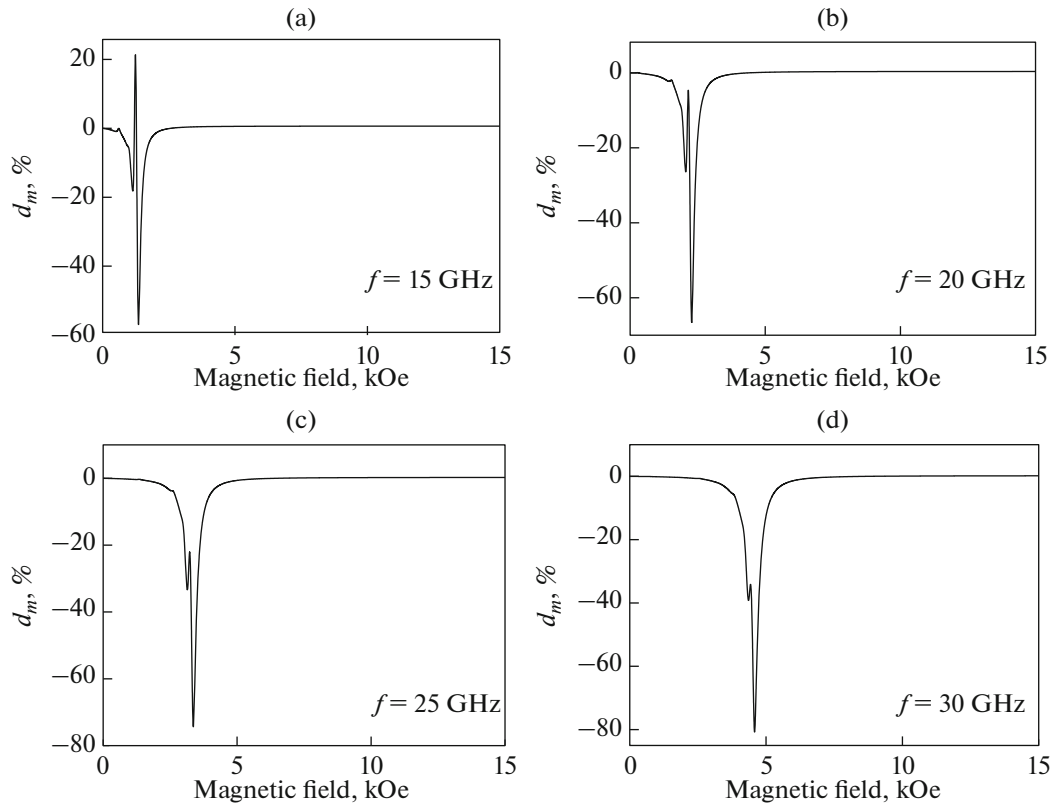
Fig. 29. Calculated dependences of the absolute value of the microwave transmission coefficient through a 290-nm-thick ferromagnetic metal plate at various frequencies: $f =$ (a) 15, (b) 20, (c) 25, and (d) 30 GHz.

both negative and positive sign. The fact that a singularity belongs to the SWR follows, in particular, from the observation that they disappear in the calculation when the spin pinning constants significantly decrease. Some of the calculation results are similar to the experimental results. The main difference between the calculation and experiment is that, in the calculation, the singularities caused by SWR are present in a wide frequency range and, in the experiment, they were detected only near the frequency $f = 36$ GHz. A comparison of the shape of the calculated and measured resonance lines is shown in Fig. 30.

It can be seen that the calculation method described above correctly reproduces the shape of the field dependence of the transmission coefficient. However, the magnitude of the resonance effects in the calculation exceeds that observed in the experiment, because only ferromagnetically ordered $Fe_{0.82}Ni_{0.18}$ layers that are a part of the cross section of the nanostructure, participate in the resonances. In addition, this model does not take into account the pinning of spins at each boundary of the layers inside the nanostructure, which leads to a weakening of the resonance singularities.

12. MICROWAVE REFRACTIVE INDEX

Knowledge of the microwave refractive index is necessary for calculating the reflection and refraction of waves at the boundaries of media and for calculating transformation of waves in electronic devices. In this section, we will calculate the refractive index from the known permittivity and permeability and consider the contributions from the FMR and μGMR phenomena, as well as the conditions under which the refractive index takes unusual values.

The complex refractive index $n_{eff} = n' - in''$ can be calculated from the known dynamic permittivity ε_{eff} and permeability μ_{eff}:

$$n_{eff} = n' - in'' = \sqrt{\varepsilon_{eff}\mu_{eff}}. \qquad (45)$$

The real part of the complex refractive index, n', represents refraction, and the imaginary part, n'', attenuation. The effective permittivity ε_{eff} in a zero external field can be determined by the methods with which modern network analyzers are supplemented. It can be determined experimentally by the transmission method [69] if, in the absence of an external magnetic field, the dynamic permeability is close to unity. In nanostructures with the GMR, the effective permittiv-
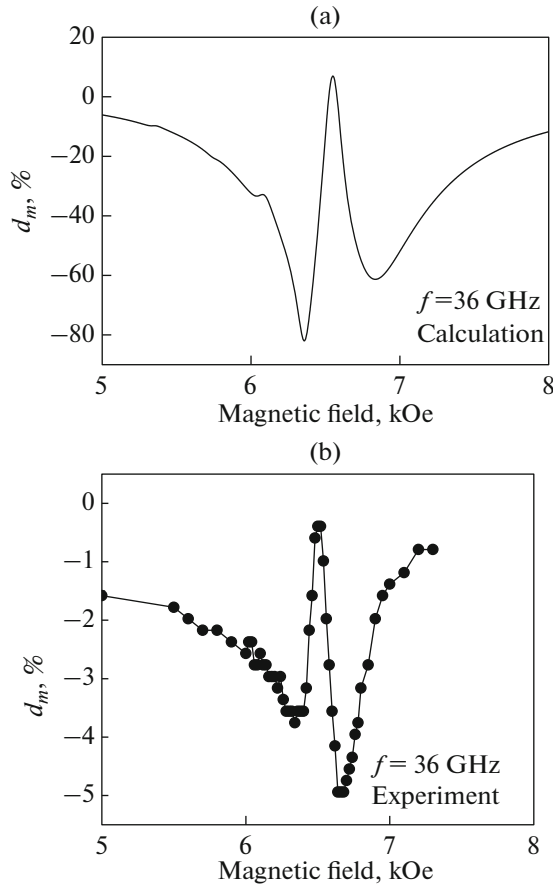
Fig. 30. (a) Calculated and (b) measured dependences of the transmission coefficient on the magnetic field at a frequency of 36 GHz.

Fig. 31. Dependences on the magnetic field of the real and imaginary parts of the refractive index for a $[Co_{88}Fe_{12}(1.3)/Cu(2.05)]_8$ superlattice at a frequency $f = 38$ GHz.

ity is a function of the magnetic field. In this case, ε_{eff} is first determined in a zero external field and then the dependence $\varepsilon_{eff}(H)$ is constructed. This method can be used in the frequency range in which equality (17) is satisfied. The dynamic permeability μ_{eff} in a zero field can be determined by the methods with which modern network analyzers are supplemented. In a magnetic field, the permeability tensor acquires off-diagonal components. To find these components and, then, μ_{eff}, one can use the results of measurements of the FMR line upon the passage of microwaves. From the linewidth, the damping factor α in the magnetic system is estimated. This estimate is not the true value of the damping factor of the substance that enters the Landau-Lifshitz equation (see [95, 102−104]). The constant α can only be used to approximate the field dependence of the permeability at a given frequency. As a rule, the approximation is performed in the approximation of the Lorentzian line shape of (8). To perform calculations, it is necessary to know the saturation magnetization of the material of the ferromagnetic layers.

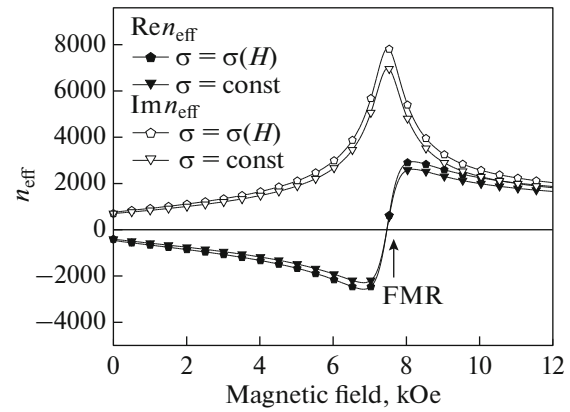First, the diagonal, μ, and off-diagonal, μ_a, components of the tensor are calculated, and then the effective permeability is determined. For example, in the case of $\mathbf{H} \perp \mathbf{H}_\sim$, the effective permeability satisfies the formula [65]

$$\mu_{eff} = \mu - \mu_a^2/\mu. \qquad (46)$$

The real part of μ_{eff} can be negative in fields smaller than the FMR field. The imaginary part is positive and has a maximum in the FMR field.

Figure 31 shows the dependences of the real and imaginary parts of the complex refractive index n_{eff} on the magnetic field for a $[Co_{88}Fe_{12}(1.3)/Cu(2.05)]_8$ superlattice at 38 GHz [120]. As can be seen from this figure, the field dependences of n_{eff} are resonant, since the field dependence of μ_{eff} is resonant. The resonance of n_{eff} coincides with the resonance of the permeability. It can be seen that the main contribution to the field dependence of the microwave refractive index is made by the FMR. However, it is possible to single out the contribution from the μGMR.

In formula (45), the μGMR exerts effect through ε_{eff}. The calculation of the refractive index n_{eff} with allowance for the magnetoresistive effect is shown in the dependences denoted as $\sigma = \sigma(H)$. In order to reveal the contribution from the GMR, a calculation was performed for the case of a constant conductivity σ = const. The adopted value of $\sigma = 3.5 \times 10^6$ S/m corresponds to the conductivity of the sample in the absence of a magnetic field. As seen from Fig. 31, the dependences at $\sigma = \sigma(H)$ and σ = const are similar, but there is a difference between the dependences, caused by the effect of the GMR on the refractive index.

Figure 31 shows that the real part of the refractive index, n', in fields smaller than the FMR field, is negative, which is determined by the inequality [121]

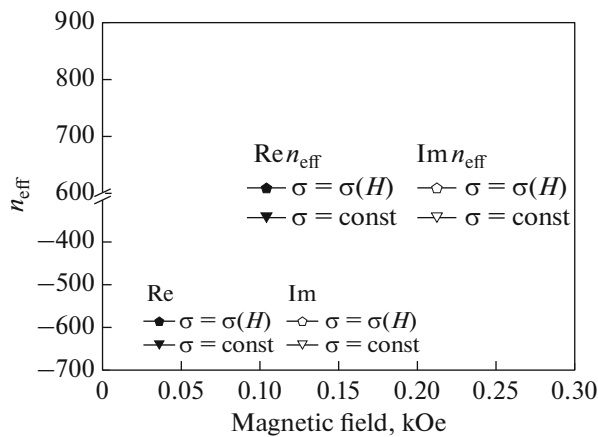$$(\varepsilon' + |\varepsilon_{eff}|)(\mu' + |\mu_{eff}|) < \varepsilon''\mu''. \qquad (47)$$

Fig. 32. Dependences of the real and imaginary parts of the refractive index on the magnetic field for a $[Co_{88}Fe_{12}(1.3)/Cu(2.05)]_8$ superlattice in the low-field region.

For a metallic object, $|\varepsilon_{eff}| \approx \varepsilon''$ and (47) reduces to the simple inequality $\mu' < 0$.

Figure 32 shows in more detail the region of fields up to 0.3 kOe, where most of the changes in the resistance of the sample occurs. Indeed, in this region of the fields, the difference between the dependences at $\sigma = \sigma(H)$ and $\sigma = const$ increases with increasing magnetic field.

13. PRACTICAL APPLICATIONS OF MICROWAVE EFFECTS IN METALLIC NANOSTRUCTURES

Attempts to utilize the GMR and μGMR phenomena began almost immediately after their discovery. A patent for a magnetic field sensor with thin antiparallel ferromagnetic layers was filed by Grünberg, the discoverer of the GMR effect, in 1990. Professor Grünberg predicted the development of electronic devices using the GMR, including spin valves. These ideas were subsequently used by IBM in hard drives. A review of the application of the GMR effect in magnetoresistive random access memory was made in 2000 [122]. As the clock frequency increased, the operating frequencies and bandwidth of computing devices also increased, moving to the GHz range.

The possibilities of using the μGMR effect in microwave devices are far from being fully realized. The variant of the arrangement of the nanostructure along the waveguide axis has certain prospects for microwave electronics. The calculation of waves in the absence of a magnetic field in such a structure is given in [70], and in an external magnetic field, in [71, 72]. On this basis, a method for contactless measurement of the high-frequency giant magnetoresistance of nanostructures was developed [73]. In [74], a nano-

structure with the GMR effect, located along the waveguide axis, is considered as the basic element of microwave electronic devices. At the next stage, we may expect the development of specific controlled devices: attenuators and phase shifters.

CONCLUSIONS

This review presents the main results of studies carried out from 1991 up to date on the transmission of microwaves through multilayer metallic nanostructures. The microwave transmission method was considered, diagrams of methods for measuring the passage of microwaves through nanostructures were given, and the measured parameters were listed. A theoretical analysis of the method was performed, the limiting cases were considered, and a comparison of the methods used by different groups was made. The results of an experimental study of the transmission of microwaves through metal nanostructures of various types have been presented. The comparison of the microwave magnetoresistive effect of the μGMR and GMR was carried out.

Various implementations of the techniques were considered, such as the microwave magnetoresistive effect in the reflection of microwaves and the microwave magnetoresistive effect with a current perpendicular to the plane of the layers of the nanostructure. Calculations of the microwave magnetoresistive effect were carried out in a wide frequency range, when the conditions of the limiting cases are not satisfied. The joint manifestation of ferromagnetic resonance and microwave magnetoresistive effect was described. Estimates of the interlayer exchange constants have been made. The manifestation of spin-wave resonance upon the passage of microwaves through a nanostructure was considered. An idea of the microwave refractive index and contributions to it from the μGMR and FMR effects has been given.

It can be concluded that the wave transmission method has become a reliable and informative method for studying metallic nanostructures. However, unresolved problems of significant interest remain. It is promising to expand the class of objects under study to nanostructures containing both ferromagnetic metal and conducting carbon layers, e.g., metal/graphene nanostructures. Of considerable interest are ferromagnetic metal/semiconductor nanostructures in which it is possible to control the properties of an electric field. In metallic nanostructures, the frequency range is expected to expand to the submillimeter-wavelength range. Of significant interest is the search for the influence of the spin-torque effect on microwave transmission and the study of ferromagnetic metal/heavy metal nanostructures to clarify the role of the Dzyaloshinskii−Moriya interaction.

FUNDING

REFERENCES

1. M. N. Baibich, J. M. Broto, A. Fert, Van Dau F. Nguyen, F. Petroff, P. Eitenne, G. Creuzet, A. Friederich, and J. Chazelas, "Giant magnetoresistance of (001)Fe/(001)Cr magnetic superlattices," Phys. Rev. Lett. **6**, No. 21, 2472−2475 (1988).

2. G. Binasch, P. Grunberg, F. Saurenbach, and W. Zinn, "Enhanced magnetoresistance in layered magnetic structures with antiferromagnetic interlayer exchange," Phys. Rev. B **39**, 4828−4830 (1989).

3. *Magnetic Nanostructures, Spin Dynamics and Spin Transport*, Ed. by H. Zabel and M. Farle (Springer, Berlin, 2013).

4. X. Zhang and W. Butler, in *Handbook of Spintronics*, Ed. by Y. Xu, D. D. Awschalom, and J. Nitta (Springer, Dordrecht, 2016).

5. A. Fert, " Origin, development and prospects of spintronics," Usp. Fiz. Nauk **178**, No. 12, 1336−1348 (2008).

6. *Ultrathin Magnetic Structures*, Ed. by B. Heinrich and J. A. C. Bland (Springer, 2005) ed. IV, Vol. 161−163, p. 257.

7. J. J. Krebs, P. Lubitz, A. Chaiken, and G. A. Prinz, "Magnetoresistance origin for nonresonant microwave absorption in antiferromagnetically coupled epitaxial Fe/Cr/Fe(001) sandwiches, J. Appl. Phys. **69**, No. 8. Pt. II, 4795−4797 (1991).

8. B. K. Kuanr, A. V. Kuanr, P. Grunberg, and G. Nimtz, "Swept-frequency FMR on Fe/Cr trilayer ultrathin films—microwave giant magnetoresistance," Phys. Lett. **221**, Nos. 3−4, 245−252 (1996).

9. V. V. Ustinov, A. B. Rinkevich, L. N. Romashev, and V. I. Minin, "Correlation between microwave transmission and giant magnetoresistance in Fe/Cr superlattice," J. Magn. Magn. Mater. **177−181**, 1205−1206 (1998).

10. J. C. Jackuet and T. Valet, *Mater. Res. Soc. Symp. Proc. Magnetic Ultrathin Films, Multilayers and Surfaces*, USA, San Francisco, (April 1995), (Pittsburgh, Pennsylvania, 1995) Vol. 384, p. 477.

11. V. V. Ustinov, A. B. Rinkevich, and L. N. Romashev, "Microwave GMR In Magnetic Metallic Multilayers," In *Giant Magnetoresistance: New Research*, Ed. by A. D. Torres and D. A. Perez, (Nova Science, 2009), p. 289.

12. V. V. Ustinov, N. G. Bebenin, L. N. Romashev, V. I. Minin, M. A. Milyaev, A. R. Del, and A. V. Semerikov, "Magnetoresistance and magnetization of Fe/Cr (001) superlattices with noncollinear magnetic ordering," Phys. Rev. B **54**, No. 22, 19958−19966 (1996).

13. P. Bruno, "Theory of interlayer magnetic coupling," Phys. Rev. B **52**, 411−439 (1995).

14. S. S. P. Parkin, R. Bhadra, and K. P. Roche, "Oscillatory magnetic exchange coupling through thin copper layers," Phys. Rev. Lett. **66**, 2152 (1991).

15. S. S. P. Parkin, "Systematic variation of the strength and oscillation period of indirect magnetic exchange coupling through the 3d, 4d, and 5d transition metals," Phys. Rev. Lett. **67**, 3598 (1991).

16. S. S. P. Parkin, N. Moore, and K. P. Roche, "Oscillations in exchange coupling and magnetoresistance in metallic superlattice structures: Co/Ru, Co/Cr, and Fe/Cr," Phys. Rev. Lett. **64**, No. 19, 2304−2307 (1990).

17. W. Kuch, A. C. Marley, and S. S. P. Parkin, "Seeded epitaxy of $Co_{90}Fe_{10}$/Cu multilayers on MgO(001): Influence of Fe seed layer thickness," J. Appl. Phys. **83**, No. 9, 4709−4713 (1998).

18. S. S. P. Parkin, "Magneto-transport in transition metal multilayered structures," *A symposium in memory of Allan Mackintosh*," Copenhagen (Denmark), 26−29 August 1996 (Matematisk-Fysiske Meddelelser, 1997) Vol. 45, pp. 113−132.

19. Y. Yang, J. -G. Zhu, R. M. White, and M. Asheghi, "Field-dependent thermal and electrical transports in Cu/CoFe multilayer," J. Appl. Phys. **99**, 063703 (2006).

20. N. S. Bannikova, M. A. Milyaev, L. I. Naumova, V. V. Proglyado, T. P. Krinitsina, I. Yu. Kamenskii, and V. V. Ustinov, "Giant magnetoresistance of CoFe/Cu superlattices with the $(Ni_{80}Fe_{20})60Cr_{40}$ buffer layer," Phys. Met. Metallogr. **116**, No.10, 1040−1046 (2015).

21. D. M. Edwards, J. Mathon, R. B. Muniz, and M. S. Phan, "Oscillations in the exchange coupling of ferromagnetic layers separated by a nonmagnetic metallic layer," J. Phys.: Condens. Matter **3**, No. 26, 4941−4958 (1991).

22. J. Bass and W. P. Pratt, "Current-perpendicular (CPP) magnetoresistance in magnetic metallic multilayers," J. Magn. Magn. Mater. **200**, 274−289 (1999).

23. A. Vedyayev, M. Chshiev, N. Ryzhanova, B. Dieny, C. Cowache, and F. Brouers, "A unified theory of CIP and CPP giant magnetoresistance in magnetic sandwiches," J. Magn. Magn. Mater. **172**, Nos. 1−2, 53−60 (1997).

24. R. E. Camley and J. Barnaś, "Theory of giant magnetoresistance effects in magnetic layered structures with antiferromagnetic coupling," Phys. Rev. Lett. **63**, No. 6, 664−667 (1989).

25. P. M. Levy, S. Zhang, and A. Fert, "Electrical conductivity of magnetic multilayered structures," Phys. Rev. Lett. **65**, No. 13, 1643−1646 (1990).

26. R. E. Camley and R. L. Stamps, "Magnetic multilayers: spin configurations, excitations and giant magnetoresistance," J. Phys.: Condens. Matter **5**, No. 23, 3727−3786 (1993).

27. T. Valet and A. Fert, "Theory of the perpendicular magnetoresistance in magnetic multilayers," Phys. Rev. B **48**, No. 10, 7099−7113 (1993).

28. V. V. Ustinov and E. A. Kravtsov, "A unified semiclassical theory of parallel and perpendicular giant magne-

toresistance in metallic superlattices," J. Phys.: Condens. Matter **7**, No. 18, 3471−3484 (1995).

29. *Molecular Beam Epitaxy and Heterostructures*, Ed. by L. L. Chang and K. Ploog (Springer, 1985).

30. S. Gangopadhyay, J. X. Shen, M. T. Kief, J. A. Barnard, and M. R. Parker, "Giant magnetoresistance in CoFe/Cu multilayers with different buffer layers and substrates," IEEE Trans. Magn. **31**, No. 6, 3933−3935 (1995).

31. M. A. Milyaev, L. I. Naumova, and V. V. Ustinov, "Exchange-coupled superlattices with record magnetoresistance," Phys. Met. Metallogr. **119**, No. 12, 1162−1166 (2018).

32. V. Lauter-Pasyuk, H. J. Lauter, B. Toperverg, O. Nikonov, E. Kravtsov, L. Romashev, and V. Ustinov, "Magnetic neutron off-specular scattering for the direct determination of the coupling angle in exchange-coupled multilayers," J. Magn. Magn. Mater. **226−230**, Part 2, 1694−1696 (2001).

33. V. Lauter-Pasyuk, H. J. Lauter, B. Toperverg, O. Nikonov, E. Kravtsov, M. Milyaev, and V. Ustinov, "Magnetic off-specular neutron scattering from Fe/Cr multilayers," Phys. B: Condens. Matter **263**, 194−198 (2000).

34. A. B. Rinkevich, D. V. Perov, E. A. Kuznetsov, and V. V. Ustinov, "Spin-wave resonance in $(Fe_{0.82}Ni_{0.18})/V$ nanostructure," J. Exp. Theor. Phys. **129**, 911−9236 (2019).

35. A. B. Drovosekov, O. V. Zhotikova, N. M. Kreines, V. F. Meshcheryakov, M. A. Milyaev, L. N. Romashev, V. V. Ustinov, and D. I. Kholin, "Inhomogeneous ferromagnetic resonance modes in [Fe/Cr]n superlattices with a high biquadratic exchange constant," J. Exp. Theor. Phys. **89**, 986−994 (1999).

36. A. B. Drovosekov, N. M. Kreines, D. I. Kholin, V. F. Meshcheryakov, M. A. Milyaev, L. N. Romashev, and V. V. Ustinov, "Ferromagnetic resonance in multilayer $[Fe/Cr]_n$ structures with noncollinear magnetic ordering," JETP Lett. **67**, 727−732 (1998).

37. S. O. Demokritov, A. B. Drovosekov, N. M. Kreines, Kh. Nembakh, M. Rikart, and D. I. Kholin, "Interlayer interaction in a Fe/Cr/Fe system: Dependence on the thickness of the chrome interlayer and on temperature," J. Exp. Theor. Phys. **95**, 1062−1073 (2002).

38. N. M. Kreines, "Investigation of interlayer interaction in magnetic multilayer structures $[Fe/Cr]_n$ by the method of ferromagnetic resonance," Fiz. Nizk. Temp. **28**, No. 8/9, 807−821 (2002).

39. A. B. Rinkevich, M. A. Milyaev, and L. N. Romashev, "Ferromagnetic resonance and interlayer exchange coupling in $(Fe/Cr)_n$ superlattices," Phys. Met. Metallogr. **120**, No. 3, 247−253 (2019).

40. M. A. Milyaev, L. I. Naumova, V. V. Proglyado, T. P. Krinitsina, A. M. Burkhanov, N. S. Bannikova, and V. V. Ustinov, "Giant changes in magnetic and magnetoresistive properties of CoFe/Cu multilayers at subnanosized variations in the thickness of the chromium buffer layer," Phys. Met. Metallogr. **112**, No. 2, 138−145 (2011).

41. A. V. Chumak, V. I. Vasyuchka, A. A. Serga, and B. Hillebrands, "Magnon spintronics," Nat. Phys. **11**, 453−461 (2015).

42. B. Divinskiy, V. E. Demidov, S. O. Demokritov, A. B. Rinkevich, and S. Urazhdin, "Route toward high-speed nano-magnonics provided by pure spin currents," Appl. Phys. Lett. **109**, No. 25 (2016).

43. S. A. Nikitov, D. V. Kalyabin, I. V. Lisenkov, A. N. Slavin, Yu. N. Barabanenkov, S. A. Osokin, A. V. Sadovnikov, E. N. Beginin, M. A. Morozova, Yu. P. Sharaevskii, Yu. A. Filimonov, Yu. V. Khivintsev, S. L. Vysotskii, V. K. Sakharov, and E. S. Pavlov, "Magnonics: A new research area in spintronics and spin wave electronics," Phys. Usp. **185**, No. 10, 1002−1028 (2015).

44. Ch. Pool, *Electron Spin Resonance. Comprehensive Treatise on Experimental Techniques* (Interscience Publishers, Wiley, New York, 1967).

45. J. Stankowski, F. Stobiecki, and M. Gorska, "Application of magnetically modulated microwave absorption to study of giant magnetoresistance effect in the Ni−Fe/Cu multilayer system," Appl. Magn. Reson. **24**, 303−311 (2003).

46. C. T. Boone, J. M. Shaw, H. T. Nembach, and T. J. Silva, "Spin-scattering rates in metallic thin films measured by ferromagnetic resonance damping enhanced by spin-pumping," J. Appl. Phys. **117**, 223910 (2015).

47. S. Mizukami, Y. Ando, and T. Miyazaki, "Effect of spin diffusion on Gilbert damping for a very thin permalloy layer in Cu/permalloy/Cu/Pt films," Phys. Rev. B **66**, 104413 (2002).

48. M. Kostylev, "Waveguide-based ferromagnetic resonance measurements of metallic ferromagnetic films in transmission and reflection," J. Appl. Phys. **113**, 053908 (1−5) (2013).

49. S. Sangita Kalarickal, P. Krivosik, W. Mingzhong, C. E. Patton, M. L. Schneider, P. Kabos, T. J. Silva, and J. P. Nibarger, "Ferromagnetic resonance linewidth in metallic thin films: Comparison of measurement methods," J. Appl. Phys. **99**, 093909 (2006).

50. R. L. Ramey and T. S. Lewis, "Properties of thin metal films at microwave frequencies," J. Appl. Phys. **39**, 1747−1751 (1968).

51. I. V. Antonets, L. N. Kotov, S. V. Nekipelov, and E. N. Karpushov, "Conducting and reflecting properties of thin metal films," Tech. Phys. **11**, 1496−1500 (2004).

52. A. B. Rinkevich, L. N. Romashev, and V. V. Ustinov, "Radiofrequency magnetoresistance of Fe/Cr superlattices," J. Exp. Theor. Phys. **90**, 834−841 (2000).

53. A. Rinkevich, A. Nossov, V. Ustinov, V. Vassiliev, and S. Petukhov, "Penetration of the electromagnetic waves through doped lanthanum manganites," J. Appl. Phys. **91**, No. 6, 3693−3697 (2002).

54. A. B. Rinkevich, L. N. Romashev, V. V. Ustinov, and E. A. Kuznetsov, "High frequency properties of magnetic multilayers," J. Magn. Magn. Mater. **254−255**, 603−607 (2003).

55. T. Rausch, T. Szczurek, and M. Schlesinger, "High frequency giant magnetoresistance in evaporated Co/Cu multilayers deposited on Si (110) and Si (100)," J. Appl. Phys. **85**, No. 1, 314−318 (1999).

56. A. B. Rinkevich and L. N. Romashev, "Non-contact measurement of microwave magnetoresistance of met-

al multilayers," Radiotekhnika i elektronika **44**, No. 5, 557−560 (1999).

57. Z. Frait, P. Sturc, K. Temst, Y. Bruynseraede, and I. Vavra, "Microwave and d.c. differential giant magnetoresistance study of iron/chromium superlattices," Solid State Commun. **112**, 569−573 (1999).

58. V. V. Ustinov, A. B. Rinkevich, L. N. Romashev, and E. A. Kuznetsov, "Reflection of electromagnetic waves from Fe/Cr nanostructures," Pis'ma Zh. Tekh. Fiz. **33**, 23−31 (2007).

59. D. E. Endean, J. N. Heyman, S. Maat, and E. Dan Dahlberg, "Quantitative analysis of the giant magnetoresistance effect at microwave frequencies," Phys. Rev. B **84**, 212405 (2011).

60. M. M. Kirillova, I. D. Lobov, V. M. Maevskii, A. A. Makhnev, E. I. Shreder, V. I. Minin, L. N. Romashev, A. V. Semerikov, A. R. Del', and V. V. Ustinov, "Optical, magneto-optical properties, and giant magnetoresistance of Fe/Cr superlattices with noncollinear ordering of iron layers," Zh. Eksp. Teor. Fiz. **109**, No. 2, 477−494 (1996).

61. I. D. Lobov, M. M. Kirillova, L. N. Romashev, M. A. Milyaev, and V. V. Ustinov, "Magnetorefractive effect and giant magnetoresistance in Fe(t_x)/Cr superlattices," Phys. Solid State **51**, No. 12, 2480−2485 (2009).

62. V. V. Ustinov, Yu. P. Sukhorukov, M. A. Milyaev, A. B. Granovskii, A. N. Yurasov, E. A. Gan'shina, and A. V. Telegin, "Magnetotransmission and magnetoreflection in multilayer Fe/Cr nanostructures," J. Exp. Theor. Phys. **108**, 260−266 (2009).

63. I. D. Lobov, M. M. Kirillova, A. A. Makhnev, L. N. Romashev, and V. V. Ustinov, "Parameters of Fe/Cr interfacial electron scattering from infrared magnetoreflection," Phys. Rev. B **81**, No. 13, 134436 (6) (2010).

64. A. B. Rinkevich, D. V. Perov, V. O. Vas'kovskii, and V. N. Lepalovskii, "Regularities of penetration of electromagnetic waves through metal magnetic films," Tech. Phys. **54**, 1339−1349 (2009).

65. A. G. Gurevich and G. A. Melkov, *Magnetic Vibrations and Waves* (Nauka, Moscow, 1994).

66. V. V. Ustinov, "High frequency impedance of magnetic superlattices showing giant magnetoresistance," J. Magn. Magn. Mater. **165**, No. 1−3, 125−127 (1997).

67. N. A. Semenov, *Technical Electrodynamics* (Svyaz', Moscow, 1972) [in Russian].

68. L. M. Brekhovskikh, *Waves in Layered Media* (Izdatel'stvo akademii nauk SSSR, Moscow, 1957) [in Russian].

69. A. B. Rinkevich, M. I. Samoilovich, S. M. Klescheva, D. V. Perov, A. M. Burkhanov, and E. A. Kuznetsov, "Millimeter-wave properties and structure of gradient Co−Ir films deposited on opal matrix," IEEE Trans. Nanotechnol. **13**, No. 1, 3−9 (2014).

70. A. B. Rinkevich, L. N. Romashev, and E. A. Kuznetsov, "Electromagnetic waves in a rectangular waveguide with a metallic nanostructure," Radiotekhnika i Elektronika **49**, No. 1, 48−53 (2004).

71. V. V. Ustinov, A. B. Rinkevich, and L. N. Romashev, "Interaction of electromagnetic waves with iron-chromium multilayer nanostructures," Tech. Phys. **50**, 484−490 (2005).

72. V. V. Ustinov, A. B. Rinkevich, L. N. Romashev, and D. V. Perov, "Giant magnetoresistance of iron-chromium superlattices at microwaves," Tech. Phys. **49**, No. 5, 613−618 (2004).

73. A. B. Rinkevich, L. N. Romashev, and E. A. Kuznetsov, "Measurement of high-frequency giant magnetoresistance of nanostructures in the traveling wave mode," Radiotekhnika i Elektronika **51**, No. 1, 93−99 (2006).

74. A. B. Rinkevich, L. N. Romashev, V. V. Ustinov, and E. A. Kuznetsov, "Rectangular waveguide with metallic nanostructure driven by magnetic field," Int. J. Infrared Millimeter Waves. **28**, 567−578 (2007).

75. A. B. Rinkevich, M. A. Milyaev, L. N. Romashev, and D. V. Perov, "Microwave giant magnetoresistance effect in metallic nanostructures," Phys. Met. Metallogr. **119**, 1297−1300 (2018).

76. V. V. Ustinov, A. B. Rinkevich, L. N. Romashev, M. A. Milyaev, A. M. Burkhanov, N. N. Sidun, and E. A. Kuznetsov, "Penetration of electromagnetic fields through multilayered and cluster-layered Fe/Cr nanostructures," Phys. Met. Metallogr. **99**, No. 5, 486−497 (2005).

77. V. V. Ustinov, L. N. Romashev, M. A. Milayev, A. V. Korolev, T. P. Krinitsina, and A. M. Burkhanov, "Kondo-like effect in the resistivity of superparamagnetic cluster-layered Fe/Cr nanostructures," J. Magn. Magn. Mater. **300**, 148−152 (2006).

78. A. B. Rinkevich, V. V. Ustinov, L. N. Romashev, M. A. Milyaev, N. N. Sidun, and E. A. Kuznetsov, "High-frequency properties of Fe/Cr superlattices with thin Cr layers in the millimeter-wavelength range," Tech. Phys. **58**, No. 7, 1073−1079 (2013).

79. V. V. Ustinov, A. B. Rinkevich, L. N. Romashev, A. M. Burkhanov, and E. A. Kuznetsov, "Giant magnetoresistive effect in Fe/Cr multilayers in a wide range of frequencies," Phys. Met. Metallogr. **96**, No. 3, 291−297 (2003).

80. D. P. Belozorov, V. N. Derkach, S. V. Nedukh, A. G. Ravlik, S. T. Roschenko, I. G. Shipkova, S. I. Tarapov, and F. Yildiz, "High-frequency magnetoresonance and magnetoimpedance in Co/Cu mltilayers with variable interlayer thickness," Int. J. Infrared and Millimeter Waves **22**, No. 11, 1669−1682 (2001).

81. S. S. P. Parkin, "Magneto-transport in transition metal multilayered structures," *A symposium in memory of Allan Mackintosh,* Copenhagen (Denmark), 26−29 August 1996 (Matematisk-Fysiske Meddelelser, 1997), Vol. 45, pp. 113−132.

82. A. B. Rinkevich, Ya. A. Pakhomov, E. A. Kuznetsov, A. S. Klepikova, M. A. Milyaev, L. I. Naumova, and V. V. Ustinov, "Microwave giant magnetoresistance in [CoFe/Cu]$_n$ superlattices with record-high magnetoresistance," Pis'ma Zh. Tekh. Fiz. **45**, 42−44 (2019).

83. B. Hjörvarsson, J. A. Dura, P. Isberg, T. Watanabe, T. J. Udovic, G. Andersson, and C. F. Majkrzak, "Reversible tuning of the magnetic exchange coupling in Fe/V(001) superlattices using hydrogen," Phys. Rev. Lett. **79**, No. 5, 901−904 (1997).

84. D. Labergerie, C. Sutter, H. Zabel, and B. Hjörvarsson, "Hydrogen induced changes of the interlayer coupling in Fe$_{(3)}$/V$_{(x)}$ superlattices ($x = 11-16$)," J. Magn. Magn. Mater. **192**, 238−246 (1999).

85. A. B. Rinkevich, D. V. Perov, E. A. Kuznetsov, M. A. Milyaev, L. N. Romashev, and V. V. Ustinov, "Microwave penetration through (Fe$_{0.82}$Ni$_{0.18}$)/V superlattices," J. Magn. Magn. Mater. **493**, 165700 (2020).

86. A. B. Granovskii, A. A. Kozlov, T. V. Bagmut, S. V. Nedukh, S. I. Tarapov, and J.-P. Clerc, "Microwave-frequency spin-dependent tunneling in nanocomposites," Phys. Solid State **47**, 738−741 (2005).

87. A. Rinkevich, L. Romashev, M. Milyaev, E. Kuztetsov, M. Angelakeris, and P. Poulopoulos, "Electromagnetic waves penetration and magnetic properties of AgPt/Co nanostructures," J. Magn. Magn. Mater. **317**, No. 1−2, 15−19 (2007).

88. V. V. Ustinov, A. B. Rinkevich, L. N. Romashev, and E. A. Kuznetsov, "Giant magnetoresistive effect and magnetic resonance in the reflection of electromagnetic waves from Fe-Cr nanostructures," Tech. Phys. **54**, 1156−1161 (2009).

89. V. V. Ustinov, A. B. Rinkevich, and L. N. Romashev, "Microwave magnetoresistance of Fe/Cr multilayers in current-perpendicular-to-plane geometry," J. Magn. Soc. Jpn. **23**, Nos. 1−2, 114−116 (1999).

90. V. V. Ustinov, A. B. Rinkevich, and L. N. Romashev, "Microwave magnetoresistance of Fe/Cr multilayers in current-perpendicular-to-plane geometry," J. Magn. Magn. Mater. **198−199**, No. 6, 82−84 (1999).

91. V. V. Ustinov, A. B. Rinkevich, L. N. Romashev, M. Angelakeris, and N. Vourttsis, "Microwave magnetoresistance of Fe/Cr superlattices for currents passing perpendicular to the plane of layers," Phys. Met. Metallogr. **93**, No. 5, 422−428 (2002).

92. J. Al'tman, *UHF Devices* (Mir, Moscow, 1968) [in Russian].

93. D. V. Perov and A. B. Rinkevich, "Frequency dependence of microwave giant magnetoresistive effect in the magnetic metallic nanostructures," Phys. Met. Metallogr. **120**, No. 4, 3333−338 (2019).

94. M. Farle, "Ferromagnetic resonance of ultrathin metallic layers," Rep. Prog. Phys. **61**, No. 7, 755−826 (1998).

95. K. Lenz, H. Wende, W. Kuch, K. Baberschke, K. Nagy, and A. Jánossy, "Two-magnon scattering and viscous Gilbert damping in ultrathin ferromagnets," Phys. Rev. B **73**, 144424 (1−6) (2006).

96. I. Neudecker, G. Woltersdorf, B. Heinrich, T. Okuno, G. Gubbiotti, and C. H. Back, "Comparison of frequency, field, and time domain ferromagnetic resonance methods," J. Magn. Magn. Mater. **307**, 148−156 (2006).

97. S. O. Demokritov, A. B. Drovosekov, D. I. Kholin, N. M. Kreines, H. Nembach, and M. Rickart, "Temperature dependence of interlayer coupling in Fe/Cr/Fe wedge samples: static and dynamic studies," J. Magn. Magn. Mater. **272−276**, 963−965 (2004).

98. N. G. Bebenin, A. V. Kobelev, A. P. Tankeyev, and V. V. Ustinov, "Magnetic resonance frequencies in multilayers with biquadratic exchange and non-collinear magnetic ordering," J. Magn. Magn. Mater. **165**, Nos. 1−3, 468−470 (1997).

99. N. G. Bebenin, A. V. Kobelev, A. P. Tankeev, and V. V. Ustinov, "FMR frequencies in multilayers with noncollinear magnetic ordering, Phys. Met. Metallogr. **82**, No. 4, 348−353 (1996).

100. A. B. Drovosekov, D. I. Kholin, N. M. Kreines, V. F. Meshcheryakov, M. A. Milyaev, L. N. Romashev, and V. V. Ustinov, "Non-uniform FMR modes in [Fe/Cr]$_n$ superlattices with strong biquadratic exchange," Fiz. Met. Metalloved. **91**, 38−41 (2001).

101. E. M. Kogan, E. A. Turov, and V. V. Ustinov, "Passage impedance of ferromagnetic metal film," Fiz. Met. Metalloved. **53**, No. 2, 223−229 (1982).

102. R. Urban, B. Heinrich, G. Woltersdorf, K. Ajdari, K. Myrtle, J. F. Cochran, and E. Rozenberg, "Nanosecond magnetic relaxation processes in ultrathin metallic films prepared by MBE," Phys. Rev. B **65**, No. 5, 020402−4 (2001).

103. R. Urban, G. Woltersdorf, and B. Heinrich, "Gilbert damping in single and multilayer ultrathin films: role of interfaces in nonlocal spin dynamics," Phys. Rev. Lett. **87**, No. 21, 217204−4 (2001).

104. R. Arias and D. I. Mills, "Extrinsic contributions to the ferromagnetic resonance response of ultrathin films," Phys. Rev. B **60**, No. 10, 7395−7409 (1999).

105. M. H. Seavey and P. E. Tannewald, "Direct observation of spin-wave resonance," Phys. Rev. Lett. **1**, No. 5, 168−169 (1958).

106. R. S. Iskhakov, S. V. Stolyar, M. V. Chizhik, and L. A. Chekanova, "Spin-wave resonance in multilayer films (one-dimensional magnon crystals). Identification rules," JETP Lett. **94**, 301−305 (2011).

107. I. G. Vazhenina, R. S. Iskhakov, and L. A. Chekanova, "Spin-wave resonance in chemically deposited fe-ni films: measuring the spin-wave stiffness and surface anisotropy constant", Phys. Solid State **60**, 292−298 (2018).

108. A. Hamadeh, O. Kelly d' Allivy, C. Hahn, H. Meley, R. Bernard, A. H. Molpeceres, V. V. Naletov, M. Viret, A. Anane, V. Cros, S. O. Demokritov, J. L. Prieto, M. Munoz, G. de Loubens, and O. Klein, "Full control of the spin-wave damping in a magnetic insulator using spin-orbit torque," Phys. Rev. Lett. **113**, 197203(1−5) (2014).

109. B. Divinsky, V. E. Demidov, S. Urazhdin, R. Freeman, A. B. Rinkevich, and S. O. Demokritov, "Excitation and amplification of spin waves by spin-orbit torque," Adv. Mater. **30**, No. 33, 1802837 (2018).

110. C. E. Patton, "Classical theory of spin-wave dispersion for ferromagnetic metals," Czech J. Phys. **26**, No. 8, 925−935 (1976).

111. B. A. Kalinikos and A. N. Slavin, "Theory of dipole-exchange spin wave spectrum for ferromagnetic films with mixed exchange boundary conditions," J. Phys. C **19**, 7013−7033 (1986).

112. V. A. Ignatchenko and R. S. Iskhakov, "Dispersion relation and spin-wave spectroscopy of amorphous ferromagnets," Zh. Eksp. Teor. Fiz. **75**, No. 4, 1438−1443 (1978).

113. N. G. Bebenin and V. V. Ustinov, "Spin waves in superlattices with biquadratic exchange," Phys. Met. Metallogr. **84**, No. 2, 112−117 (1997).

114. N. G. Bebenin and V. V. Ustinov, "Spin-wave frequencies in a superlattice with biquadratic exchange in a magnetic field," Phys. Met. Metallogr. **89**, No. 3, 225−229 (2000).

115. R. E. De Wames and T. Wolfram, "Spin-wave resonance in conducting films: parallel resonance," Jpn. J. Appl. Phys. **13**, No. 1, 68−78 (1974).

116. W. S. Ament and G. T. Rado, "Electromagnetic effects of spin wave resonances in ferromagnetic metals," Phys. Rev. **97**, No. 6, 1558−1566 (1955).

117. M. I. Kaganov and L. Yui, "Influence of the boundary condition for the magnetic moment on the spin-wave resonance in a metal," Izv. AN SSSR. Cer. Fiz. **25**, No. 11, 1375−1378 (1961).

118. A. B. Rinkevich, D. V. Perov, and V. O. Vaskovsky, "Types of magnetic resonances in electromagnetic wave penetration through thin magnetic films," Phys. Scr. **83**, 015705(13) (2011).

119. D. V. Perov, A. B. Rinkevich, and S. O. Demokritov, "Eigenmodes in thin ferromagnetic film under ferromagnetic resonance and spin-wave resonance conditions at different spin pinning," Phys. Scr. **91**, 025802(14) (2016).

120. A. B. Rinkevich, D. V. Perov, E. A. Kuznetsov, and M. A. Milyaev, "Changes in the microwave refractive index caused by the giant magnetoresistive effect," Dokl. Phys. **64**, No. 8, 316−318 (2019).

121. A. D. Boardman, N. King, and L. Velasco, "Negative refraction in perspective," Electromagnetics **25**, 365−389 (2005).

122. J. Daughton, "Magnetoresistive Random Access Memory (MRAM)," https://www.nve.com/Downloads/mram.pdf/ Copyright © 2/4/2000.

Translated by E. Chernokozhin